Nanoscale

MINIREVIEW

View Article Online
View Journal | View Issue

CrossMark click for updates

Cite this: *Nanoscale*, 2016, **8**, 9944

Multi-component superstructures self-assembled from nanocrystal building blocks

Rui Tan,† Hua Zhu,† Can Cao and Ou Chen*

More than three decades of intensive study to make high-quality nanocrystals have created a unique toolbox for building multi-component superstructures, which have been recognized as a new generation of metamaterials important to both fundamental sciences and applied technologies. This minireview summarizes recent advances in this exciting field. We will focus our discussion on the synthetic strategies and superstructures of this multi-component metamaterial, and highlight their novel properties and potential applications. Additionally, some perspectives on possible developments in this field are offered at the end of this review. We hope that this minireview will both inform and stimulate research interests for the design and fabrication of these nanocrystal-based multi-component metamaterials for diverse applications in the future.

Received 27th February 2016,
Accepted 15th April 2016

DOI: 10.1039/c6nr01662f

www.rsc.org/nanoscale

Published on 18 April 2016. Downloaded by Brown University on 18/05/2016 14:35:03.

1. Introduction

Multi-component superstructures (MCSs) self-assembled from more than one type of building blocks represent a new pathway for generating complex materials with potential for use in various technological applications.[1–4] Since the first experiments on the self-assembly of single-type nanocrystals (NCs) into superstructures in 1989,[5] inorganic NCs, with wide tunability in their size, shape and composition and easy-to-handle colloidal states, have become arguably the most popular construction material for these higher-ordered architectures.[6–11] However, early attempts to make MCS using NC building blocks often resulted in amorphous or short-range-ordered structures mainly due to uncontrollable driving forces, polydispersity of the building blocks, or both.[12–17] Recent advances in synthetic methods have produced NCs with an unprecedented high quality (*i.e.*, high monodispersity, uniform morphology, and well-controlled surface state),[18–23] and have provided methods for controlling the driving forces affecting self-assembly processes.[24–30] These substantial achievements led to the ordered and programmable self-assembly of multiple types of NCs with distinct nature into complex superstructures in the nano-, meso-, and macro-scales.[31–36]

Department of Chemistry, Brown University, 324 Brook St., Providence, RI 02912, USA. E-mail: ouchen@brown.edu
†These authors contributed equally to this work.

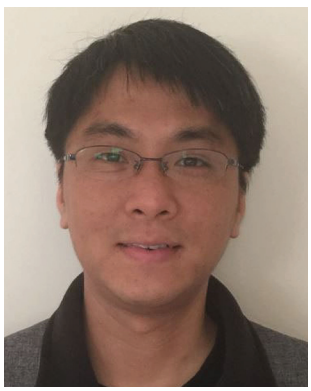

Rui Tan

Rui Tan is currently a post-doctoral associate in Professor Ou Chen's research group in the Department of Chemistry at Brown University. He received his B.S. degree in chemical physics from University of Science and Technology of China in 2006, and his PhD in chemistry from University of South Carolina in 2015. His research concentrates on quantum dot synthesis, shape control and optical property optimization. His other scientific interests include the synthesis of doped nanoparticles and self-assembly of nanocrystals.

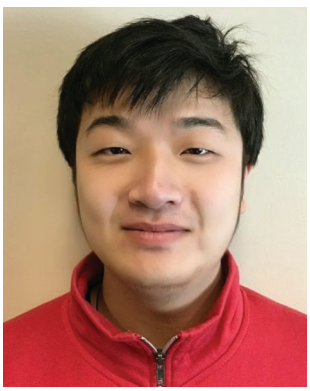

Hua Zhu

Hua Zhu obtained his B.S. degree in chemistry in 2015 from Fudan University, Shanghai, China. He is now a PhD candidate at Brown University. His research interests include the synthesis and characterization of multifunctional nanomaterials, as well as finding their potential applications.

This journal is © The Royal Society of Chemistry 2016

Published on 18 April 2016. Downloaded by Brown University on 18/05/2016 14:35:03.

By fine-tuning NC size ratios and concentrations, the first successful example of a long-range ordered binary-superlattice (BN-SL) self-assembled from Fe_2O_3 magnetic NCs and PbSe quantum dots (QDs) was demonstrated in 2003.[8] Since then, this research area has truly bloomed: currently, a wide range of MCSs including 2-dimensional (2D) membranes/films, 3-dimensional (3D) solids/supercrystals and high-order colloidal particles have been successfully synthesized.[25,34] These MCSs can not only combine or enhance the size-dependent properties of their constituents but also manifest novel interactions and synergistic properties from the near-field coupling that occurs between neighboring building blocks.[12,32,37,38]

Although there are many excellent reviews covering NC building blocks and self-assembled superstructures including synthetic methodologies, driving forces, properties and applications,[31,32,39–45] reviews specifically focused on the system of MCSs from colloidal inorganic NCs are few and in high demand. This minireview provides a great opportunity to summarize recent achievements in this fast-growing field. Our discussion will range from general synthetic strategies to current superstructures to highlight how MCSs have collective and synergistic properties that derive from their individual building blocks as well as their specific geometric arrangements. We will place a greater emphasis on supercrystalline superstructures with a long-range ordered periodicity. Note that template-based multi-component assemblies and heterostructure NCs synthesized through epitaxial or non-epitaxial crystal growth are generally not examined. Finally, challenges and future perspectives on this topic will conclude this review.

2. Synthetic strategies

From a general thermodynamic viewpoint, ensemble NCs arrive at equilibrium when Helmholtz free energy (F) is minimized. F is composed of two parts, the internal energy (U) and the product of temperature (T) and entropy (S). Thus, F is determined by both entropy and intermolecular forces between NCs, including van der Waals interactions,[46] dipole–dipole interactions,[24] electrostatic interactions,[25–27] *etc*. In this section, we will describe synthetic strategies for generating MCSs broadly classified into two categories: (1) spontaneous formation mainly dependent on solvent evaporation; (2) guided formation controlled by surface chemistry.

2.1 Spontaneous formation

Spontaneous formation processes that rely on solvent evaporation represent a strategy without pre-designed interparticle interactions to guide the formation of superstructures. As the solvent evaporates, the interparticle distance in the solution decreases, eventually to a point where the system can undergo a transition from a disordered state to an ordered structure.[40,41] This can be seen as a process of minimizing the total entropy, where the gain in free volume entropy outweighs the loss in configurational entropy, thus creating an overall increase of entropy in the system.[28,29,47–51] During this process, colloidal NCs can spontaneously self-assemble on certain solid substrates (*e.g.*, alkyl-functionalized silicon chips, silicon nitride membranes or transmission electron transmission (TEM) grids), forming periodically ordered SLs.[28,29,52] Murray *et al.* recently refined this strategy by the self-assembly of NC BN-SL membranes at a liquid/air interface.[35] In this procedure, a chemically inert liquid surface (*e.g.*, diethyl glycol) substituted for solid substrates with a glass slide to control the evaporation rate (Fig. 1a). Various NCs of selected sizes and concentrations were dissolved in a low-boiling-point solvent (*e.g.*, hexane) and then dispensed over the liquid surface. Within minutes, a floating NC-SL membrane was formed at the liquid surface as the solvent evaporated (Fig. 1a). This improved method yields centimeter-scale uniform SL membranes, which are transferrable to various substrates to make NC-based devices.[53–55]

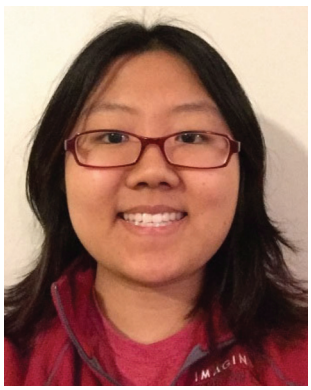

Can Cao

Can Cao is part of the Program for Liberal Medical Education class of 2018/2022 at Brown University. She is concentrating in chemistry and economics. She has been a part of Professor Ou Chen's research lab since sophomore fall semester and enjoys working with nanoparticles.

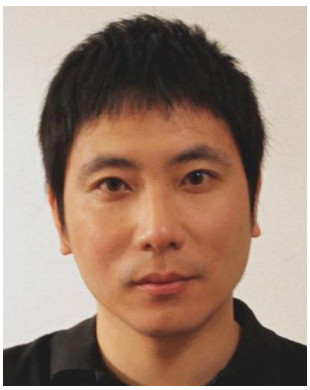

Ou Chen

Ou Chen is an Assistant Professor in the Department of Chemistry at Brown University. He received his BS degree in chemical physics from the University of Science and Technology of China (USTC) in 2004, and completed his PhD studies in the Department of Chemistry at the University of Florida. He was a postdoctoral associate working with Prof. Moungi Bawendi at MIT. His current research interests focus on the development of novel methods for synthesizing and characterizing nanocrystals and self-assembled superstructures and exploring their novel properties and potential applications.

Published on 18 April 2016. Downloaded by Brown University on 18/05/2016 14:35:03.

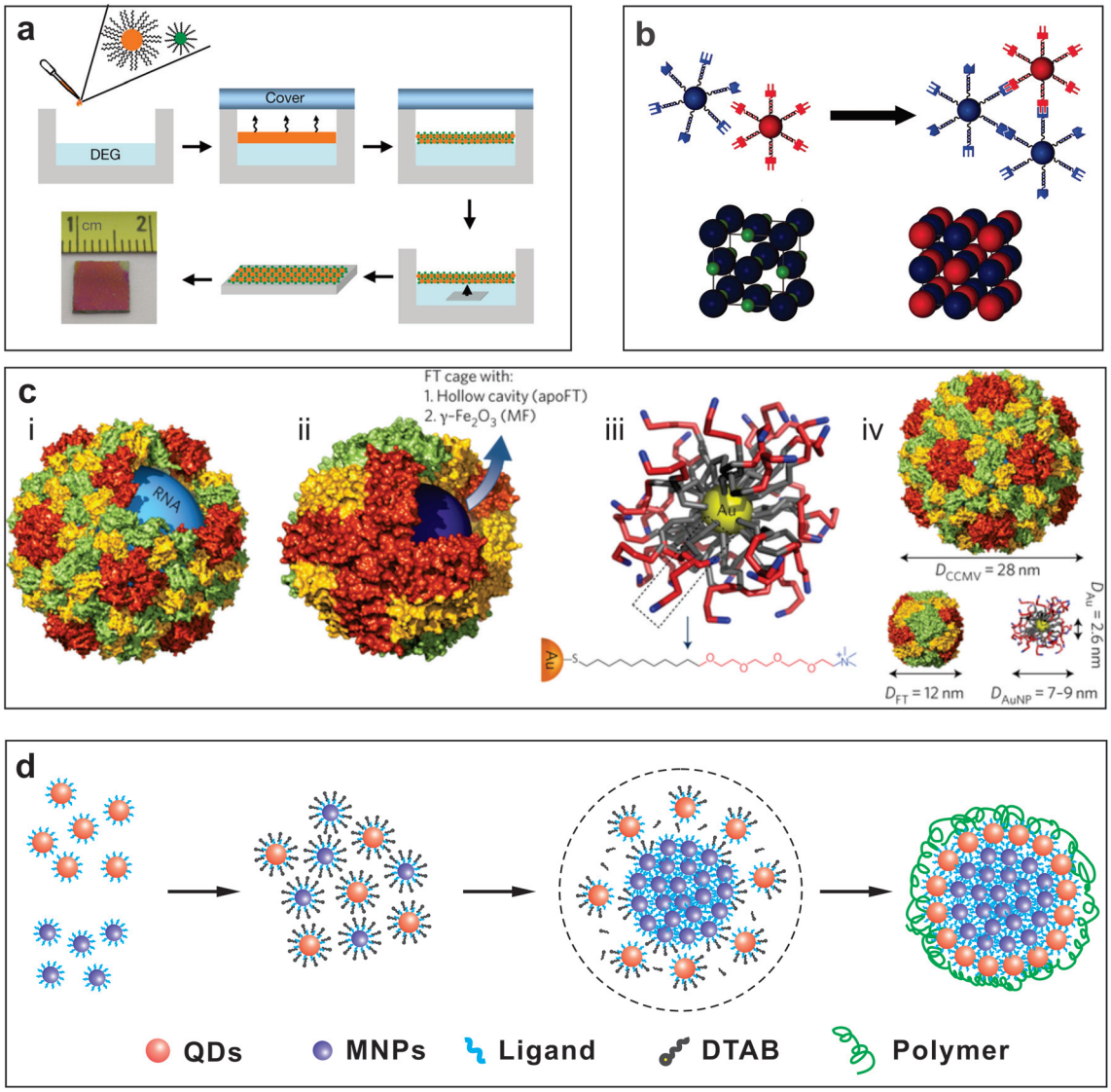

Fig. 1 (a) Schematic of the BN-SL membrane growth and transfer processes. The photograph shows a typical BN-SL membrane transferred to a SiO_2–Si wafer. Mechanical damage from tweezers in the membrane's upper right corner (photo) helps visualize the scale. (b) Complex nanoparticle assemblies can be created when programming multivalent DNA-NC interactions. For example, by encoding multiple distinct sticky end sequences on NCs, both self-complementary and non-self-complementary interactions can be used to assemble lattices. Bottom: this strategy can be used to create a NaCl lattice. (c) Materials used for the assembly of binary protein cage–nanoparticle superlattices. (i) Native cowpea chlorotic mottle virus with RNA genome inside. (ii) Apoferritin and magnetoferritin (recombinant ferritin cage from *Pyrococcus furiosus* encapsulating Fe_3O_4–g-Fe_2O_3). (iii) Au NCs stabilized with an amphiphilic ligand featuring a cationic quaternary amine end-group. (iv) Size of the building blocks drawn to scale. (d) Schematic of the formation of core–shell SPs using solvophobic interactions. Reproduced with permission from ref. 27 and 34–36.

There are several parameters that can determine the superstructure from this spontaneous formation process. For instance, temperature is one of the key parameters. On the one hand, with proper manipulation of the temperature, one can control the solvent evaporation rate; on the other hand, as the temperature increases, entropy becomes the dominant force controlling the superstructure, favoring high packing density.[28] This trend was generally observed by Talapin *et al.* in a variety of BN NC systems.[29]

In addition to the temperature effect, NC surface ligands also play a pivotal role when assembling to MCSs.[56–58] The deformability of the hydrocarbon ligand capping layer can lead to a change in the local coordination environment, which is pivotal in BN-SL packing. An important parameter, "softness" (L/R = length of surface ligand/inorganic core radius), determines whether they will adopt the shape of a coordination environment (L/R > 0.33) or follow the sphere packing rules (L/R < 0.33).[59] Pileni *et al.* studied the influence of the ligand-type and showed that the assembly of NCs with different surface ligands (*i.e.*, oleylamine and dodecanethiol) experienced a ligand exchange process.[60] This process created a large energetic penalty and affected the thermodynamic

 This journal is © The Royal Society of Chemistry 2016

Published on 18 April 2016. Downloaded by Brown University on 18/05/2016 14:35:03.

stability during assembly, leading to a remarkable change in the resulting BN structures.[60] These structures favored a kinetically trapped state with a minimum local free energy even when the packing density was low.[60]

2.2 Guided formation

In contrast to the spontaneous process, specific NC surface-to-surface interactions or surface-to-solvent interactions play a dominant role in the process of guided formation of MCSs. The controlled surface interactions in recent studies include the complementary interactions aided by DNA molecules and electrostatic interactions.[26,27,33,34,61] Complementary forces from the hydrogen bonding between different bases in DNA are specifically oriented, which allows programmable engineering of DNA-based MCSs.[62–64] Mirkin *et al.* have summarized six design rules for preparing distinct colloidal crystal structures using DNA-functionalized NCs (DNA-NCs).[34,63] It is noted that in a BN system, the size ratio between two different DNA-NCs and the DNA linker ratio, defined as the number of linkers on two different DNA-NCs, determine the thermodynamically favored structure.[34]

Early studies primarily focused on Au NC systems because they readily attached to alkylthiol-modified DNA strands. Mirkin *et al.* recently expanded this method to other NC systems by coating NCs with an azide-bearing amphiphilic polymer, which can be linked to DNA by 'azide–alkyne click chemistry'.[63] Gang *et al.* provided an alternative strategy to form heterogeneous structures of NC-SLs by using DNA and carboxylic-based interactions.[38] After grafting with carboxylic groups, streptavidin was conjugated and attached to biotinylated-DNA. Four representative functional NCs can be assembled into desired superstructures using this strategy.[38]

Aside from using DNA ligands, electrostatic interactions alone can also guide the formation of BN superstructures.[13,26,65] This strategy usually relies on controlling electrostatic attraction between NCs with opposite-charged surface layers.[65] The key to this strategy lies in a balance between positively and negatively charged NCs and a proper control of the electrolyte concentration and pH.[26,27] Recently, Kostiainen *et al.* successfully encapsulated RNA and magnetic γ-Fe_2O_3 NCs with negatively charged cowpea chlorotic mottle virus and ferritin protein cages and formed superstructures by applying positively charged Au NCs (Fig. 1c).[27] The crystallinity of these structures strongly depended on the Debye screening length as well as the solution pH.

Furthermore, guided MCS formation can also arise from surface-to-solvent interactions.[66–69] Solvophobic interactions occurring between nonpolar ligands on NC surfaces and polar solvent molecules can be used for synthesizing colloidal superparticles (SPs).[70–75] Recently, Chen *et al.* refined this strategy to form multi-component SPs using Fe_3O_4 NCs and CdSe/CdS core/shell QDs as building blocks.[36] As shown in Fig. 1d, a mixture of hydrophobic NCs was first transferred to an aqueous solution using dodecyltrimethylammonium bromide (DTAB) as a surfactant. The resulting micelle solution was injected into a poly(vinylpyrrolidone) ethylene glycol solution. The weakened van der Waals interactions between ligands and surfactants lead to the detachment of DTAB surfactants from the NC surface, introducing solvophobic interactions between ligands and solvent molecules. To minimize the total surface area and surface energy, NCs tend to aggregate to form SPs. Interestingly, a phase separation occurred inside each SP during this process. 'Core–shell' SPs with a magnetic NC 'core' and a fluorescent QD 'shell' were attained (Fig. 1d).[36]

3. Diverse superstructures

Utilizing the strategies described above, a large number of MCSs with different structures and compositions have been successfully developed over the last decade. Since early observations on BN-SL self-assembly of Au and Ag NCs by Kiely *et al.*,[9,76] the library of MCSs has been continuously expanding to various systems including 2D membranes,[25,52,77] 3D SL solutions,[34,63,78,79] dried solids[26,62,80] and multi-component SPs.[36,67,68] In this section, we will summarize this diverse structure library of MCSs with an emphasis on their supercrystallinity.

3.1 2D-SL membranes

Primarily through the spontaneous formation processes previously discussed, a wide range of multi-component 2D-SLs have been achieved and demonstrated in the past ten years. Table 1 summarizes recent developments in the formation of 2D-SL membranes with different structures and building blocks. For example, Murray *et al.* have successfully assembled and summarized 12 different types of thermodynamically stable and long-range ordered BN-SLs using metal, metal oxide and semiconductor NCs (Fig. 2a–l).[25,52,77] Also in their studies, three 'undefined' BN-SLs assembled from LaF_3 triangular nanoplates and spherical NCs (Au or PbSe) and three 'unknown' BN-SLs assembled from Pd–PbSe, Ag–Fe_3O_4, and Au–Fe_3O_4 spherical NCs have been discovered.[25,52] After these early studies, BN-SL membranes have expanded into various NC systems with diverse structures including isostructural NaCl,[81] CuAu,[82,83] NiAs,[81] AlB_2,[81,82,84] $MgZn_2$ [57,82,84] and $NaZn_{13}$ [51,81,82,84,85] types, *etc.* Ye *et al.* have carried out a more systematic study and revealed that pure bcc-AB_6 type BN-SL assembled *via* Fe_3O_4 and Au NCs can be formed under slow evaporation.[86] During this process, the relative phase stability of bcc-AB_6 and CaB_6 can be tailored from coexistence to phase-pure bcc-AB_6 by adjusting the NC size ratio. After an early demonstration of isostructural cesium chloride (CsCl) using poly(methyl methacrylate) particles,[87] the same structure has been obtained in BN-SLs from PbSe and CdSe QDs with a particle size ratio as high as 0.75.[28]

In addition to the BN-SLs formed from a combination of metallic, magnetic and semiconductor NCs, Pileni *et al.*, observed BN-SLs using purely metal constituents.[88] They showed that the variation of size ratio of Co and Ag NCs from 1/8 to 1 will change the structure from $NaZn_{13}$ to a mixture of AlB_2 and AuCu, and finally to AlB_2 owing to the strong van der Waals interactions between metal NCs.[88,89] In contrast, using a single size ratio of inorganic cores, various BN-SLs including

Published on 18 April 2016. Downloaded by Brown University on 18/05/2016 14:35:03.

Table 1 Summary of recent reported 2D multi-component SL superstructures

	Isostructure/ stoichiometry	Particle shape	Building blocks (large–small NCs)	Size ratio[b]	Surface ligand	Remarks
Binary[25,52]	AB: NaCl, CuAu, Orthorhombic AB	Spherical, triangular	Fe_2O_3–Au; PbSe–Pd	0.43[a]; (0.528[a], 0.62[a])	OA; DDT; ADA, HAD	Summary and characterizations of more than 20 types of BN-SLs.
			PbSe–Ag; PbSe–Au	0.59; (0.66; 0.81)		
	AB_2: AlB_2, $MgZn_2$, $MgNi_2$		PbSe–Ag; PbS–Pd	0.71[a]; 0.56[a];		
	AB_3: Cu_3Au		$CoPt_3$–Fe_2O_3; Fe_2O_3–PbSe	0.54[a]; 0.5[a]		
	AB_4: Fe_4C		PbSe–Au	0.787[a]		
	AB_5: $CaCu_5$		PbSe–Pd	(0.6[a]; 0.48)		
	AB_6: CaB_6		PbSe–Ag	0.59		
	AB_{13}: $NaZn_{13}$, cub-AB_{13}		PbSe–Pd; PbSe–Ag	0.52; 0.58		
	"Unknown": 3 types[52]		PbSe–Ag; PbSe–Au	0.57; 0.69		
	"Undefined": 3 types[25]		Fe_2O_3–Au	0.37;		
			PbSe–Pd; PbSe–Ag	0.63[a]; 0.662[a]		
			PbSe–Pd; Fe_2O_3–Ag; Fe_2O_3–Au	0.48; 0.31; 0.37		
			LaF_3–Au; LaF_3–Au; LaF_3–PbSe	0.55; 0.55; 0.69		
Binary[37]	NaCl, CuAu	Spherical	PbTe–Ag_2Te; Ag_2Te–PbTe	0.49 0.64	OA, DDT	BN-SLs with enhanced p-type conductivity.
Binary; ternary[54]	AB, AB_2 A_2B_3, AB_3 ABC_2	Spherical	Fe_3O_4–Au; Fe_3O_4–FePt (NaFY$_4$:Yb/Er)–Fe_3O_4 Fe_3O_4–Fe_3O_4–FePt	0.44[a]; 0.40[a]; 0.49[a]; 0.63[a]; 0.42[a]; 1 : 0.48 : 0.37[c]	OA	2D BN-SLs; bilayer BN-SLs; TN-SLs.
Quasi-quaternary[55]	$NaZn_{13}$, AlB_2	Spherical	(CdSe/ZnS/CdS)–(Au/Fe_3O_4); (CdSe/ZnS)–(Au/Fe_3O_4); (PbSe/CdSe)–(Au/Fe_3O_4)	0.48 0.33 0.45	OA, OAm, HAD, DDT	Quasi-quaternary AB_{13}- and AB_2-type SLs for the first time using exclusively core/shell NCs.
2D Binary; (3D binary)[57]	$NaZn_{13}$, AlB_2, $AuCu_3$, bcc-AB6 ($C_{60}K_6$, $C_{60}Cs_6$) NaCl, $MgZn_2$, $CaCu_5$, AB_8, AB(CsCl), A_2B_3	Spherical	Fe_3O_4–polymer-grafted Au	0.49[a] 0.49[a] 0.40[a] 0.69[a] 0.49[a]	OA, TP, CP	10 different BN-SLs formed by polymer-grafted NCs.
Binary[60]	NaCl, AlB_2, $NaZn_{13}$, $MgZn_2$	Spherical	Au, (w/different sizes)	0.43[a]; 0.57[a] 0.57[a]; 0.82[a]	OAm	Ligand coverage, solvent type dependent stability.
Polymorphism binary[77]	ico-AB_{13}, cub-AB_{13}	Spherical	PbSe–Pd	0.627[a]; 0.671[a]; 0.595[a]	OA, DDT	Identify AB_{13} polymorph.
			Fe_3O_4–PbSe	0.520[a]		
Quasi-ternary[81]	NaCl, NiAs, AlB_2, AB_{13}, $NaZn_{13}$, cub-AB_{13}	Spherical	Fe/Fe_3O_4(core/shell)–Au	0.44[a]	OA, OAm	TN-SLs with high packing density.
Binary[84]	AlB_2, $MgZn_2$, $CaCu_5$, cub-$NaZn_{13}$, ico-$NaZn_{13}$	Spherical	CdTe–CdSe CdTe–Au	0.57[a], 0.63[a] 0.71[a], 0.81[a]	DDT	Size ratio dependent BN-SLs.
Binary[85]	AB_2, cub-AB_{13}	Spherical	PbSe–CdSe	0.56[a]	TOPO, HDA, OA	QD BN-SLs.
Binary[86]	CaB_6, bcc-AB_6	Spherical	Fe_3O_4–Au	0.43[a]	DDT	Identify AB_6 polymorph.
Binary[88]	NaCl, AlB_2, AuCu, $AuCu_3$, $NaZn_{13}$	Spherical	Co–Ag	0.49[a]; 0.49[a]–0.59[a]; 0.54[a]–0.67[a]	OA, DDT	Concentration ratio led to structure change.
Binary[89]	$MgZn_2$, $NaZn_{13}$	Spherical	Co–Co; Co–Ag	0.76[a]; 0.59[a]	OA, DDT	Magnetic dipolar interactions.
Binary[90]	A_6B_{19}: $[PbSe]_6[CdSe]_{19}$	Spherical	PbSe–CdSe	0.61–0.67	OA, HDA	New structure, A_6B_{19}-type.
Quasi-binary[91]	$AB_{3.86}$-type	Spherical	PbS–Pd, Fe_2O_3–Au	0.43[a]	OA, DDT	Identification of quasicrystalline order BN-SLs.

This journal is © The Royal Society of Chemistry 2016

Published on 18 April 2016. Downloaded by Brown University on 18/05/2016 14:35:03.

Table 1 *(Contd.)*

	Isostructure/ stoichiometry	Particle shape	Building blocks (large–small NCs)	Size ratio[b]	Surface ligand	Remarks
Binary[95]	AB_2-type	Rod, spherical	$NaYF_4$–Fe_3O_4; CdSe–Au; $NaYF_4$–UO_2; CdSe–Pd	(0.56, 0.29)[d] (1.12, 0.32)[d] (0.38, 0.19)[d] (0.92, 0.26)[d]	OA,	Formation of AB_2 BN-SLs with NCs of rod and spherical shape.
Binary; ternary[98]	AC_2: AlB_2 BC_2: $MgZn_2$ ABC_4: $AlMgB_4$	Spherical	PbSe–CdSe PbSe–CdSe PbSe–PbSe–CdSe	0.48 0.73 1 : 0.65 : 0.48	OA, HDA	Observation of TN-SLs with ABC_4-type.
Binary, ternary[99]	AB, AB_2, AB_6, ABC	Disk, rod	LaF_3–(CdSe/CdS) LaF_3–LaF_3–(CdSe/CdS)	0.40[a]; 0.25[a] 1 : 0.40 : 0.25[a]	OA	BN-SLs and TN-SLs with NCs of disk and rod shape.
Binary[116]	$NaZn_{13}$, $MgZn_2$	Spherical	$CoFe_2O_4$–Fe_3O_4	0.53; 0.74	OA	BN-SLs with bistable magnetoresistance switching behavior.
Binary[138]	ico-AB_{13}	Spherical	Silica (15 nm, 29.1 nm)	0.52	—	Silica BN-SLs.
Binary[139]	NaCl, $CaCu_5$, AlB_2, $NaZn_{13}$, bcc-AB_6, quasicrystals	Spherical	{Mo_{132}}–PbS[e]; {Mo_{132}}–CdSe[f]; {Mo_{132}}–(PbS/CdS); {$Mo_{72}V_{30}$}–PbS	(0.41[a], 0.51[a], 0.58[a], 0.74[a])[e] 0.49[a,f] 0.46[a,f] 0.68[a,f]	DDA, OA	POM/NC. BN-SLs.
Binary[140]	AB	Spherical	Mo_{132}–(γ-Fe_3O_4)	0.63[a]	DDA, DODA, OA	BN-SLs preserving magnetic properties.
Binary[141]	$NaZn_{13}$, CsCl	Spherical	Co–Ag	0.73	OA, DDT	$CoAu_{13}$ BN-SLs with high thermal stability.
Binary[142]	AB_6	Spherical	Fe_3O_4–PbSe	0.32	OA	BN-SLs formed *via* controlled fusion of hexamer NC clusters.
Binary[143]	Simple hexagonal AB_2	Spherical	Si–Au	0.527[a]	DD, DDT	First Au/Si BN-SLs.

[a] Effective size ratio. [b] NC size ratio, small/large. [c] Determined by $d_{eff} = d_{core} + 2d_{shell}$, size ratio $\gamma = d_{small}/d_{large}$.[54] [d] Size ratio indicated by (diameter of sphere/diameter of rod, diameter of sphere/length of rod). [e] All five structures and quasicrystals can be formed for {Mo_{132}}–PbS with γ = 0.41–0.74. [f] AlB_2, $NaZn_{13}$, and quasicrystals can be formed for {Mo_{132}}–CdSe with γ = 0.49; AlB_2 structure formed for {Mo_{132}}–(PbS/CdS) with γ = 0.46 and for {$Mo_{72}V_{30}$}–PbS with γ = 0.68. DODA: dioctadecyldimethylammonium; TOPO: trioctylphosphine oxide; DD: dodecene; OA: oleic acid; DDT: dodecanethiol; HDA: hexadecylamine; DDA: dodecyldimethylammonium; POM: polyoxometalate clusters; TP: thiol-terminated polystyrenes; CP: carboxyl-terminated polystyrenes.

new structural types such as the AB_8-type and the A_2B_3-type can be obtained by using polystyrene-grafted NCs as building blocks.[57] These polymeric ligands offer a new method to precisely tune the properties of NC building blocks in more dimensions (*e.g.*, molecular weight, chemical nature, architecture, *etc.*). Finally, a new structure with a $[PbSe]_6[CdSe]_{19}$ (A_6B_{19}) stoichiometry, which has no direct counterpart in the atomic world, has been discovered in BN-SL membranes (Fig. 2m).[90]

Aside from periodic order, Archimedean tiling-based aperiodic ordering and dodecagonal quasi-crystalline (DDQC) superstructures can also be achieved by self-assembling colloidal NCs.[30,91,92] For instance, Talapin *et al.* observed different DDQC BN-SLs assembled *via* intermediate NC concentration ratios following the general sphere-packing rules (Fig. 2n).[91] When using ferromagnetic single domain (hcp) Co NCs instead of amorphous-phase Co particles to assemble Co–Ag BN-SLs, Pileni's group showed that the DDQC order could be obtained as a result of Co–Co magnetic dipole–dipole interactions.[30]

In addition to spherical building blocks, multi-component membranes assembled from anisotropic shaped NCs have also been explored.[25,93] For example, 2D arrays of spherical NCs (*i.e.*, Au, PbSe, Pd NCs) intercalated with parallelly aligned CdSe/CdS nanorods in the presence of suitable additive ligands were observed by Cao *et al.*[94] A mechanistic study suggested that spherical NCs with a high dielectric constant and a large Hamaker constant played important roles during this kinetically limited formation process. Lately, it has been demonstrated that self-assembly of $NaYF_4$ nanorods and Fe_3O_4 nanospheres induced at the liquid–air interface could form highly ordered NC BN-SLs into several unprecedented phases including long-range ordered AB_2-type (Fig. 2o and p).[95] Three key factors have been identified for such formation, including attractive contact interactions and optimal interaction strengths as well as suitable particle geometries which allow dense packing to maximize entropic forces.[95] NCs with other shapes, such as triangular, octahedral, rhombic, tripodal and nanoplate, have all been realized in SL membranes through shape complementary geometries and attractive contact interactions at optimal interaction strengths.[96,97]

Knowledge accumulated through studying unary and binary systems has led to several successes in making quasi-ternary and ternary-superlattice (TN-SL) membranes.[54,81,98,99] Vanmae-

Published on 18 April 2016. Downloaded by Brown University on 18/05/2016 14:35:03.

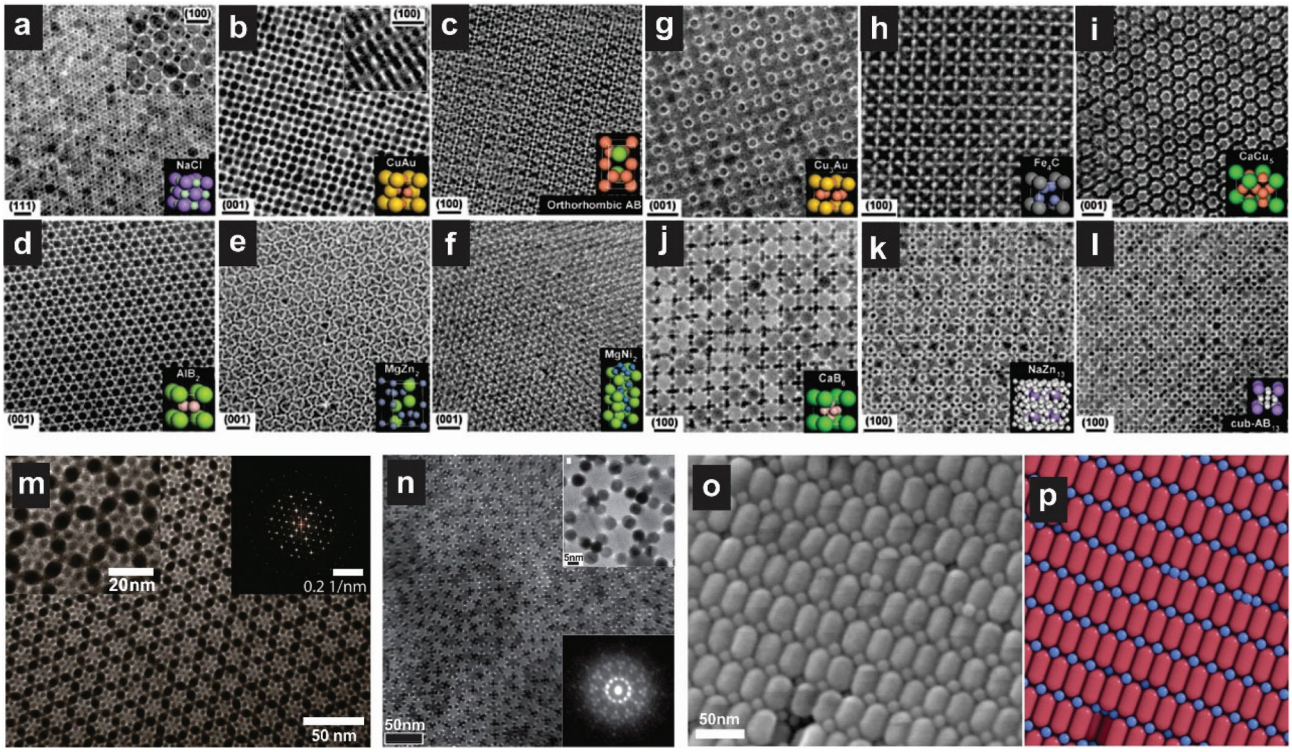

Fig. 2 (a–l) TEM images of the characteristic projections of BN-SLs, self-assembled from different NCs and modeled unit cells of the corresponding 3D structures. (m) TEM image of NC-SL obtained in a particle size ratio 0.61-0.67 with a hexagonal symmetry. (n) TEM image of a quasicrystalline SL self-assembled from 13.4 nm Fe_2O_3 and 5 nm Au NCs. Inset: top, magnified view of a dodecagonal nanoparticle quasicrystal; bottom, selected-area electron diffraction pattern with non-crystallographic 12-fold rotational symmetry measured from a ~6 μm^2 domain. (o) SEM images of the rod–sphere self-assembled from $NaYF_4$ nanorods and 11.0 nm Fe_3O_4 nanospheres and (p) compared with a theoretical reconstruction. Scale bars: (a–c), (e), (f), (i–l) 20 nm; (d), (g), (h) 10 nm. Reproduced with permission from ref. 25, 90, 91 and 95.

kelbergh *et al.* reported the first observation of genuine TN-SLs (*i.e.*, ABC_4) constructed from CdSe QDs and PbSe QDs of two different sizes with a maximum packing fraction as low as 0.64.[98] Later, bilayered ABC_2-type TN-SLs assembled from three spherical NCs and ABC-type TN-SLs assembled from small and large LaF_3 nanodisks and CdSe/CdS nanorods at a liquid–air interface were obtained by Murray *et al.*[54,99] These studies further enriched the knowledge base on SL membranes and opened the door to even more complex 2D architectures.

3.2 3D superstructures

Beyond 2D membranes, 3D MCS research has also developed quickly within the last ten years.[26,100–102] While many studies focused on single-component 3D SLs, various 3D MCSs including bulk SL solutions,[34,79,103–105] dried nanosolids,[26,62,80] and meso-scale SPs[36,67,68] have been successfully synthesized.

After early studies of applying DNA oligonucleotides as a programmable ligand to form short-range ordered assemblies,[7,62,80,106,107] Mirkin *et al.* utilized these ideas in the assembly of 3D BN-SL solutions using DNA-Au NCs of different sizes as well as hollow spherical nucleic acids as "3D spacers".[34,78] By independently tuning the oligonucleotide interconnection length, NC inorganic size, and NC hydrodynamic radius, 3D BN-SL isostructures with CsCl, NaCl, AlB_2, Cr_3Si, and Cs_6C_{60} were obtained.[34,78] Very recently, highly crystalline 3D BN-SLs have been successfully assembled by mixing two types of DNA-NCs such as CdSe/ZnS QDs, Au, Fe_3O_4 and Pt NCs with a shell of nucleic acids (Fig. 3).[63] Other structures, such as AB_8^{fcc}-type and AB^{sc}-type 3D BN-SLs, can be assembled by taking advantage of electrostatic forces between two oppositely charged NCs in solutions.[27] This concept also applies to assemblies with two types of oppositely charged proteins such as cowpea chlorotic mottle virus and amine-terminated generation six poly(amidoamine) dendrimer or cowpea chlorotic mottle virus and avidin to yield new structures (*e.g.*, AB_{12}^{bcc}).[61]

Furthermore, as in 2D membrane systems, DNA assisted self-assemblies can overcome the limitations of unary and binary systems to allow the formation of 3D TN-SL solutions.[79] Recent discoveries demonstrated a strategy for the topotactic insertion of a second component into a unary parent SL to form a BN-SL or a third component into a binary parent SL to form a TN-SL. Two unique 3D BN-SLs (A_2B_3-type and AB_4-type, both have no atomic equivalent) and three distinct 3D TN-SLs crystal structures were synthesized, such as face-perovskite type and edge-perovskite type as well as ABC_{12}-type which has no equivalent in atomic or molecular crystals.[79] Additionally, such SL switching by intercalation has proved to be a reversible process controlled by temperature.[79]

Aside from studies on 3D SL solutions, significant developments have occurred in the formation of dried nano-

 This journal is © The Royal Society of Chemistry 2016

Published on 18 April 2016. Downloaded by Brown University on 18/05/2016 14:35:03.

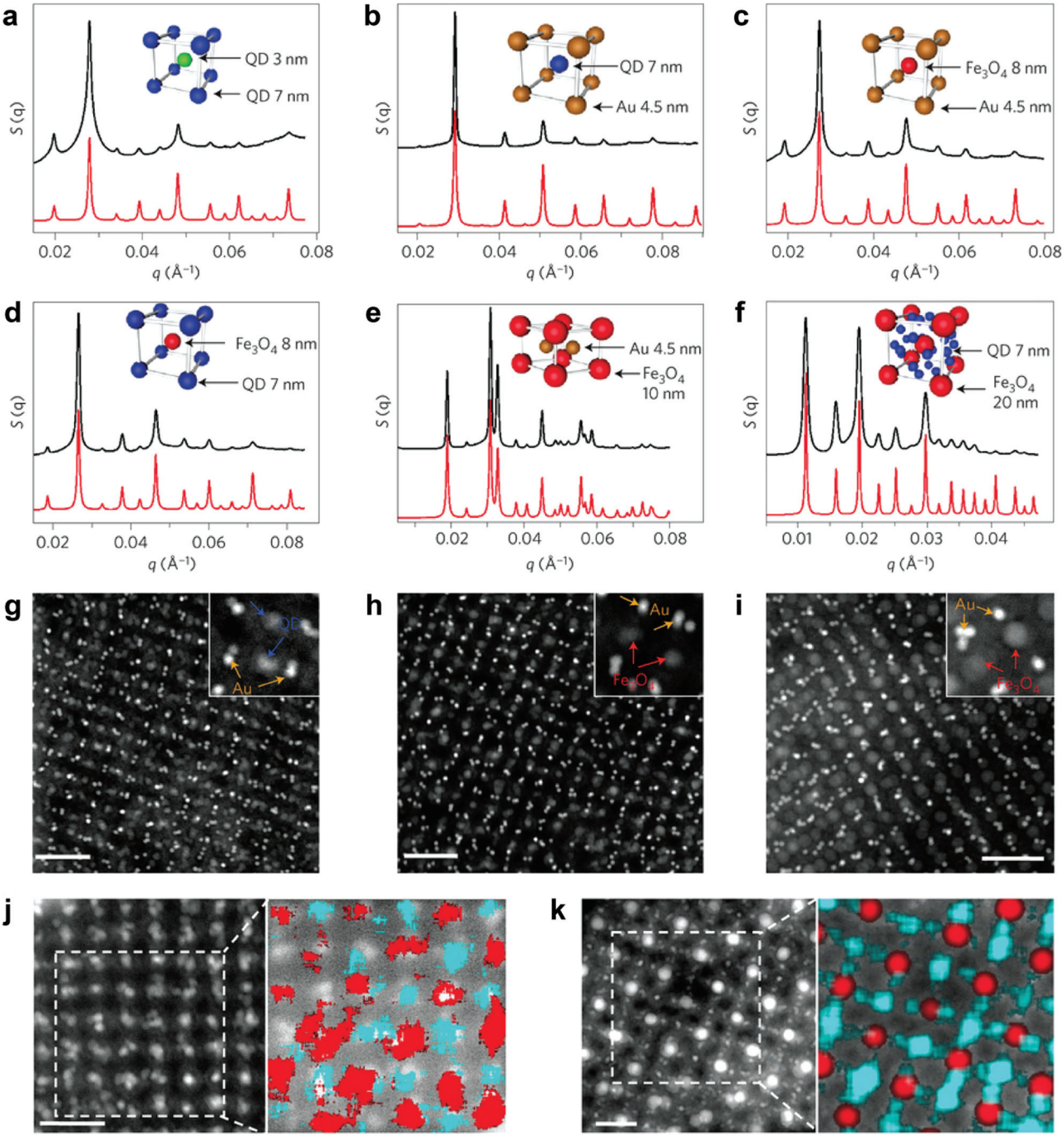

Fig. 3 BN-SLs assembled from arbitrary combinations of QD-, Au- and Fe_3O_4-programmable atom equivalents. (a–f) SAXS data for: 7 nm QD, 3 nm QD CsCl lattices (a); 7 nm QD, 4.5 nm Au CsCl lattices (b); 8 nm Fe_3O_4, 4.5 nm Au CsCl lattices (c); 8 nm Fe_3O_4, 7 nm QD CsCl lattices (d); 10 nm Fe_3O_4, 4.5 nm Au AlB_2-type lattices (e); and 20 nm Fe_3O_4, 7 nm QD Cs_6C_{60}-type lattices (f). Experimental data are shown in black, and predicted scattering patterns are shown in red. (g–i) STEM images of 7 nm QD, 4.5 nm Au CsCl lattices (g); 8 nm Fe_3O_4, 4.5 nm Au CsCl lattices (h); and 10 nm Fe_3O_4, 4.5 nm Au AlB_2-type lattices (i). Insets at the right corner are higher-magnification images with labels denoting particle composition. (j) and (k) STEM images and EDX maps of 8 nm Fe_3O_4, 7 nm QD CsCl lattices (j), and 20 nm Fe_3O_4, 7 nm QD Cs_6C_{60} lattices (k). In EDX maps, the signal from Fe is shown in red, and the signal from Cd is shown in cyan. All scale bars are 50 nm. Reproduced with permission from ref. 63.

solids.[26,62,80] Kalsin and co-workers demonstrated that mixing a solution of positively charged Au NCs and negatively charged Ag NCs coated with ω-functionalized alkane thiols will cause aggregation into binary crystals with diamond-like lattices including octahedral, truncated and twinned octahedral, truncated tetrahedral and triangular crystal morphologies.[26] Also, through a slow cooling of two different sizes of complementary DNA-Au NCs, rhombic dodecahedron shaped microcrystals

Published on 18 April 2016. Downloaded by Brown University on 18/05/2016 14:35:03.

(thermodynamically the most favorable crystal shape) with a CsCl lattice symmetry can be produced.[62] More recently, novel 3D binary nanosolids composed of two different shapes of Au NCs were successfully assembled; examples include cube–sphere binaries with NaCl-like lattices as shown in Fig. 4 and octahedron–sphere binaries with CsCl-like lattices.[80]

3D MCSs also include meso-scale colloidal SPs. Several groups have successfully synthesized multi-component SPs using NC building blocks with different compositions including metals, metal oxides, semiconductors and lanthanides.[67,68,108–110] However, producing monodispersed multi-component SPs with supercrystallinity is still a challenge. Recently, Chen *et al.* have developed a size-controlled synthesis of monodispersed multi-component 'core–shell' SPs through solvophobic interactions as previously mentioned. Additional thermal annealing treatment transformed the amorphous magnetic 'core' into a face-centered-cubic (fcc) supercrystalline structure, while preserving the 'core–shell' superstructure (Fig. 5).[36] Other types of multi-component SPs such as a planet–satellite structure with an Au NC surrounded by multiple QDs have also been achieved.[111,112] Further extensions including structures with controlled planet–satellite distances, stoichiometries, and arrangements of satellite NCs have also been reported.[113–115]

4. Novel properties

The fundamental advantage of assembling multi-component NCs into a single construct is the possibility of creating materials with novel and enhanced properties. These pro-

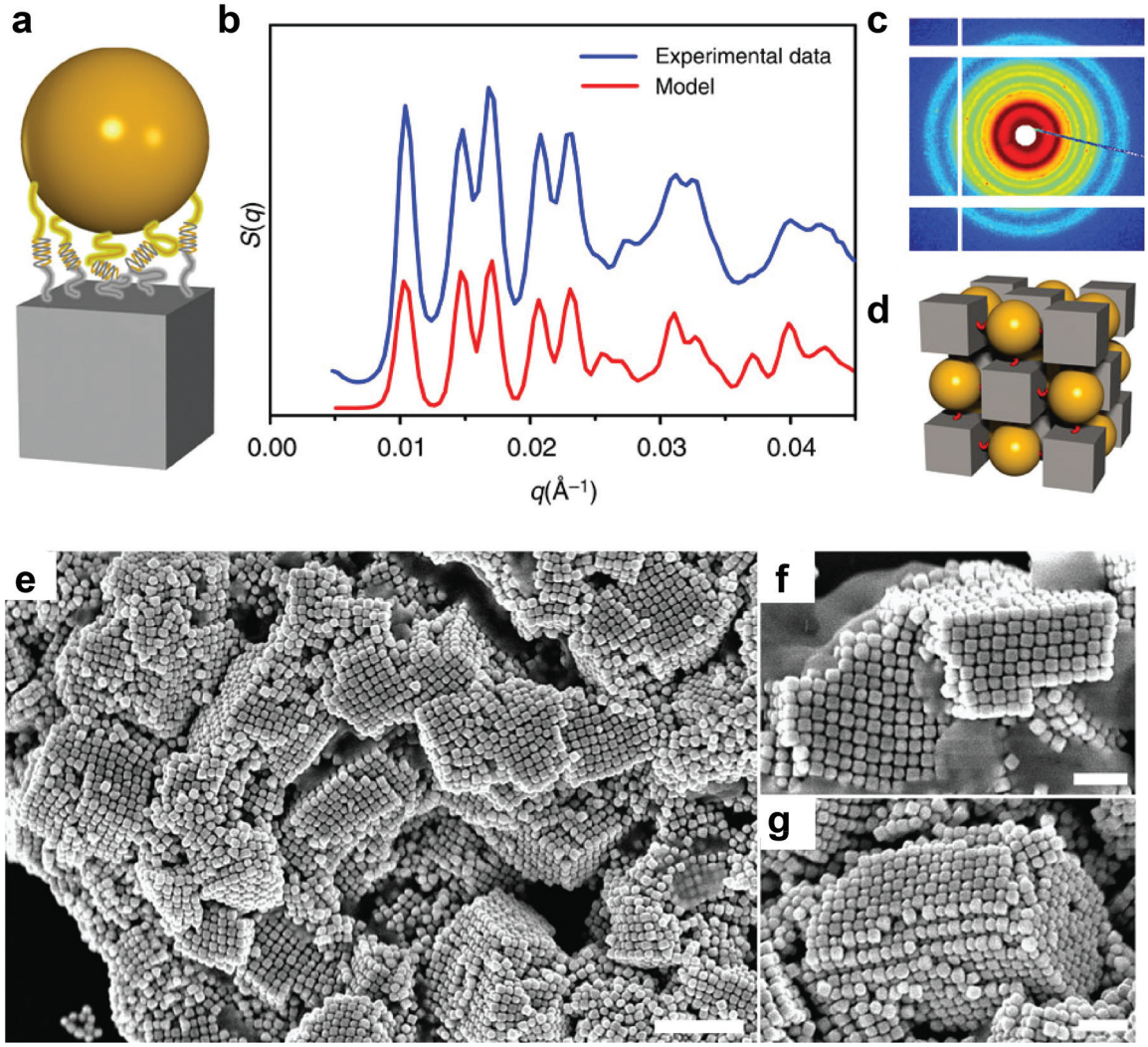

Fig. 4 Cube–sphere NC assemblies of SLs. (a) Schematic of a 46 nm spherical NCs/46 nm cube (CB) pair linked by DNA. (b) SAXS data with experimental (blue) and modelled (red) structure factors, $S(q)$, (c) scattering image and (d) the corresponding structure schematic for the 46 nm SNP/46 nm CB assembly system, which crystallizes into a NaCl-type lattice with a space group symmetry of $Fm\bar{3}m$. (e) Low-magnification SEM image of SNP/CB-assembled crystals, where square-lattice ordering can be observed from the fragments, even though drying effects caused cracks in the crystals (scale bar, 500 nm). (f) and (g) High-magnification images of the superlattice, demonstrating the alternate packing of SNPs and CBs in the 3D square lattice (scale bar, 200 nm). Reproduced with permission from ref. 80.

 This journal is © The Royal Society of Chemistry 2016

Published on 18 April 2016. Downloaded by Brown University on 18/05/2016 14:35:03.

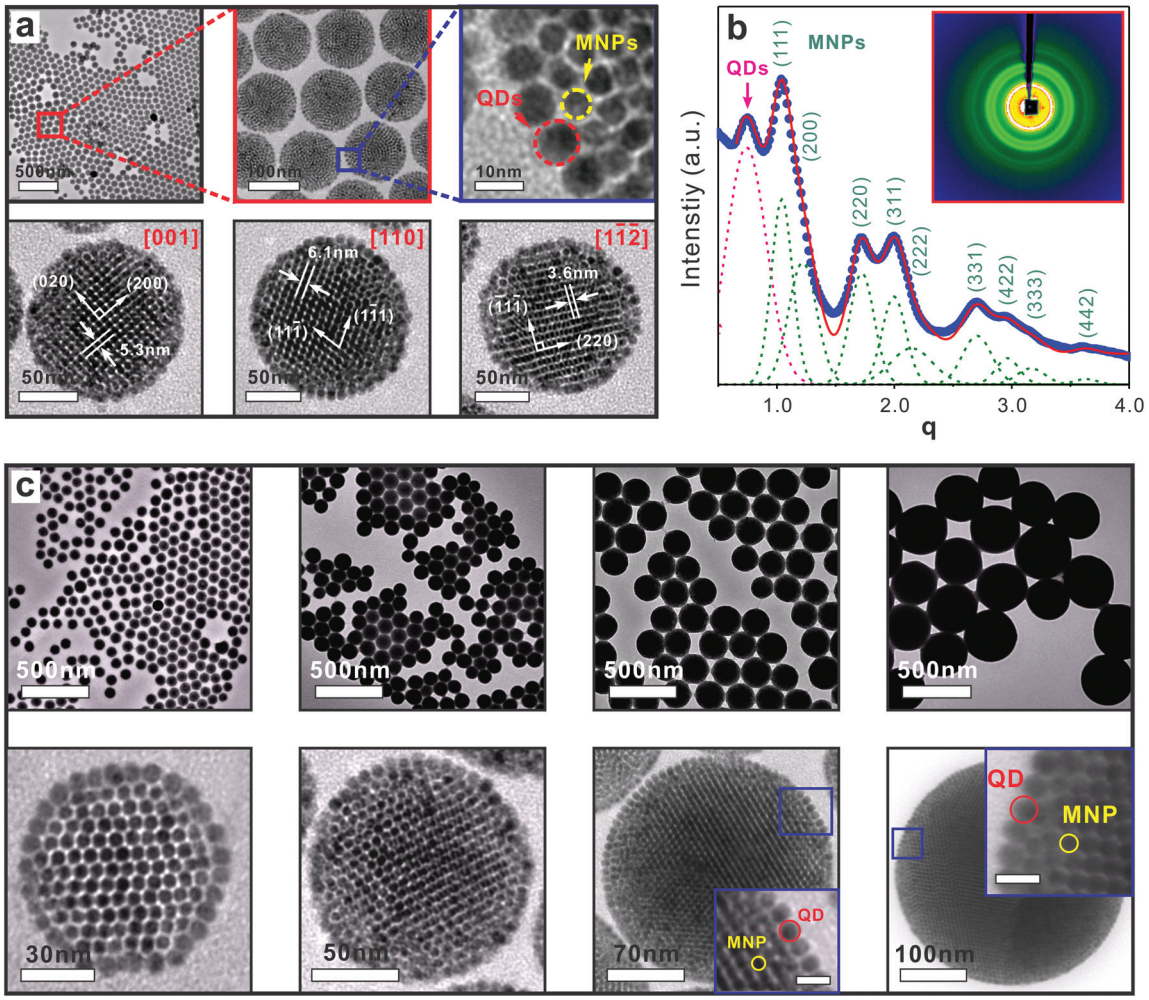

Fig. 5 (a) TEM images of core–shell SPs (CS-SPs) at different magnifications and supercrystalline CS-SPs viewed along different zone axes [001], [110] and [11$\bar{2}$]; (b) the integrated data from the SAXS pattern (inset) of CS-SPs show a position ratio series of $q/q_0 = 1/\sqrt{4/3}/\sqrt{8/3}/\sqrt{11/3}/\sqrt{4}/\sqrt{19/3}/\sqrt{8}/\sqrt{9}/\sqrt{12}$ (q_0 is the position of the (111) peak, $q = 4\pi\sin\theta/\lambda$), indicating an fcc close packing of the MNPs. (c) Large-area and higher magnification TEM images of CS-SPs. Reproduced with permission from ref. 36.

perties can be introduced from not only individual components for their size-dependent nature, but also from novel collective and synergistic properties induced by NC attachments, interparticle interactions and superstructure geometries. These enhanced functionalities make MCS materials viable in diverse areas including energy and data storage, catalysis, and biological and biomedical imaging. In this section, we will explore the number of great discoveries that have been made in this field.

4.1 Film conductivity

Inspired by the high electronic conductivity and low thermal conductivity of Ag^+ p-doped bulk CdTe, Urban *et al.* have demonstrated an enhanced conductivity effect by assembling Ag_2Te and PbTe NCs into BN-SL thin films,[37] thus overcoming the difficulty of conventional semiconductor atomic doping processes. Inside this binary film, the Ag_2Te NCs played the role of a p-type nano-dopant in the PbTe NC-SL membrane. After hydrazine treatment to replace the bulky organic ligands and to decrease interparticle distances, the p-type electronic conductivity of the film showed ~100-fold enhancement in an AB BN-SL (stoichiometry ratio of 1 : 1), compared to films made from the individual components (Fig. 6).[37] This study demonstrates a clear advantage of designing and combining multi-type NCs into metamaterials.

4.2 Magnetic coupling

Strong exchange coupling and/or dipole–dipole interactions that originate from interparticle interactions and finite crystal size effects will occur inside magnetic NC assemblies. Exchange coupling effects in short-range ordered FePt–Fe_3O_4 binary nanocomposite magnets were firstly reported by Sun *et al.*[12] Murray *et al.* further improved the same system into a long-range ordered BN-SL. They showed that the AB_2-type BN-SL membranes exhibited a temperature-dependent higher magnetoresistance value than the ico-AB_{13}-type ones.[116] This

Published on 18 April 2016. Downloaded by Brown University on 18/05/2016 14:35:03.

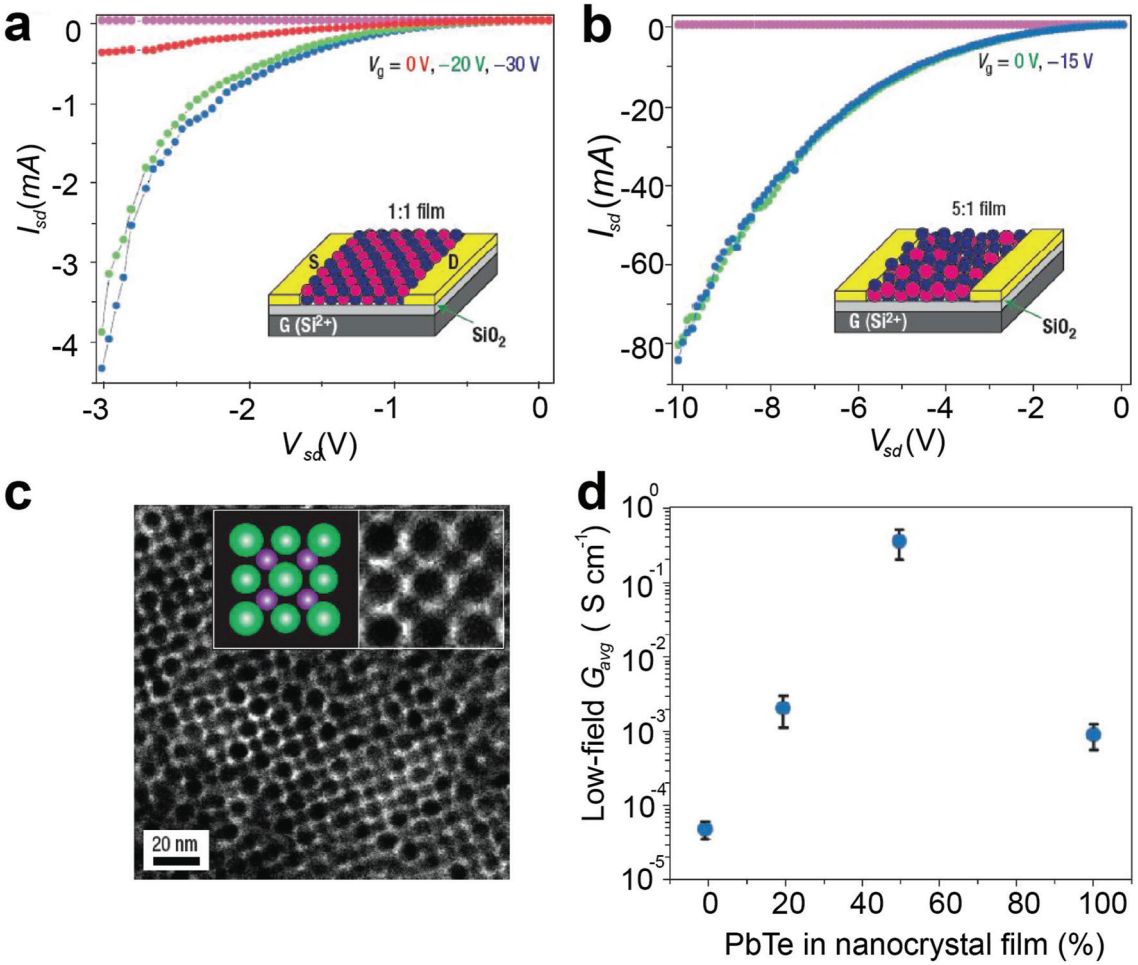

Fig. 6 Characterization of binary PbTe–Ag_2Te NC films. All measurements were recorded in forward and reverse to assess device hysteresis. Gate currents (magenta) are also plotted to demonstrate that no current leakage occurred through the gate oxide. These gate currents (I_g *versus* V_{sd}) are recorded in parallel for each I_{sd} *versus* V_{sd} measurement at every gate voltage; however, owing to the low Ig values they seem collinear. (a) *I–V* measurement of 1 : 1 PbTe–Ag_2Te binary-NC film demonstrating high p-type conductivity and no gate response. (b) *I–V* measurement of a 5 : 1 PbTe–Ag_2Te binary NC film, again demonstrating p-type transport and no gate response. (c) TEM micrograph of a 1 : 1 PbTe–Ag_2Te SL after heat treatment, demonstrating that even 200 °C thermal treatments under vacuum do not abrogate SL order. (d) Comparison of average low-field conductances (not exceeding 10 V in source–drain or 15 V in gate voltage) calculated over at least 12 devices for pure Ag_2Te films, pure PbTe films, binary 1 : 1 PbTe–Ag_2Te films and binary 5 : 1 PbTe–Ag_2Te films. The average conductances for these compositions are 5.1×10^{-5} S cm^{-1}, 9.21×10^{-4} S cm^{-1}, 0.346 S cm^{-1} and 0.0021 S cm^{-1}, respectively. The error bars are the standard deviations in conductance values for each of the compositions. These data demonstrate the synergistic enhancement of conductivity manifest in the binary-NC solids. Reproduced with permission from ref. 37.

difference was attributed to their different SL structures. Based on these discoveries, a later more systematical study on magnetic thin films was carried out by the same group. They revealed that by combining magnetically hard (*i.e.*, $CoFe_2O_4$) and soft (*i.e.*, Fe_3O_4) NCs, a single-phase magnetization switching behavior can be observed at temperatures below 200 K after annealing at 400 °C.[116] When annealed at a higher temperature (*i.e.*, 500 °C), $NaZn_{13}$-type BN-SLs exhibited a larger magnetoresistance switching field even at room temperature, which is essential for constructing nonvolatile memory chips.[116] Furthermore, when thermally stable NCs (*e.g.*, MnO NCs) were used to prevent the sintering of FePt NCs, the obtained BN-SL membranes were preserved even at 650 °C, which allowed the FePt NCs to go through a crystal phase conversion process from superparamagnetism (fcc) to ferromagnetism (face-centered-tetragonal, fct).[53] This offers a new route for the production of ferromagnetic NC arrays for high-density magnetic recording technology.

4.3 Catalytic activity

In addition to the enhanced conductivity and novel magnetic coupling, several groups have recently reported improved catalytic activities offered by MCS systems.[56,58,96,115,117] Yamada *et al.* applied the novel concept of a 'tandem' bilayer of Pt and CeO_2 NCs on a silica substrate for catalysis reactions.[56] Two sequential reactions of methanol decomposition and ethylene

 This journal is © The Royal Society of Chemistry 2016

Published on 18 April 2016. Downloaded by Brown University on 18/05/2016 14:35:03.

hydroformylation were selectively catalyzed at CeO_2–Pt and Pt–SiO_2 interfaces, respectively. By assembling a variety of noble-metal NCs on metal–oxide (*e.g.*, CeO_2 and TiO_2) NC supporting materials, mesoporous multi-component SPs can serve as thermally stable catalysts with good selectivity and robust performance for reactions at temperatures up to 500 °C.[108] Furthermore, an excellent example showing a unique advantage of the geometric control of MCSs has been reported by Kang *et al.*[96] They demonstrated that Pd–Pt BN-SL electrocatalysts show 4–6 times greater activity in the oxygen reduction reaction than pure Pt octahedral NCs or a Pt–Pd NC random mixture (Fig. 7).[96] The Pd-promoted Pt catalysts were selectively assembled from 6 nm spherical Pd NCs on highly exposed (111) facets of Pt octahedral NCs in an ico-AB_{13} BN-SL structure (Fig. 4a–c). This specific binary geometry is believed to be responsible for the observed synergistic effect.[96] Thus, as demonstrated by these studies, long-range ordered supercrystalline structures represent a more efficient and customizable method to fabricate catalysts capable of high performance and multi-functionality.

4.4 Optical and plasmonic interactions

When optical and plasmonic NCs approach each other, strong exciton and plasmonic interactions as well as synergistic phenomena are expected. Initial optical studies showed that by directly assembling Au NCs and CdSe QDs into four different types of binary superstructures, the photoluminescence of CdSe QDs dramatically decreased.[82] This observation was attributed to the energy transfer from the exciton of QDs to the plasmon resonance of Au NCs due to the close contact between the QDs and Au NCs. Shortened QD photoluminescence lifetimes further supported this hypothesis, indicating that the radiative decay rate of the exciton was significantly influenced by the surrounding Au NCs.[82] Later studies reported that by separating QDs from Au NCs using different spacers (*e.g.*, DNA, organic molecule, silica, *etc.*), a plasmon induced photoluminescence enhancement, which has long existed at the single particle level,[118–120] was observed in ensemble 3D Au NC and QD colloidal assemblies.[38,111–113,121]

In addition to the exciton–plasmonic interactions, strong near-field plasmonic–plasmonic resonances can be achieved in BN-SLs as the interparticle distances between metal NCs decrease. For the first time, Ye *et al.* successfully tuned the collective plasmonic response in BN-SLs self-assembled by plasmonic NCs (*i.e.*, Au and Ag NCs), and nonplasmonic NCs (*i.e.*, Fe_3O_4, PbS and PbTe NCs).[122] By adjusting the NC arrangement, and therefore the strength of near-field coupling between plasmonic NCs, the corresponding extinction spectra can be easily tuned across the entire visible region.

Apart from the assemblies of metal, metal oxide and semiconductor QDs, lanthanide-doped rare earth NCs (*e.g.*, $NaYF_4$: Yb,Tm,Er) with upconversion emission behavior have also been used to make binary and bilayer SLs.[54,123] Their upconversion emissions were well-preserved in a monolayer, and superimposed in bilayer SLs without any spectrum shift, which is appealing for creation of multicolor ultraviolet emission photonic devices.[123]

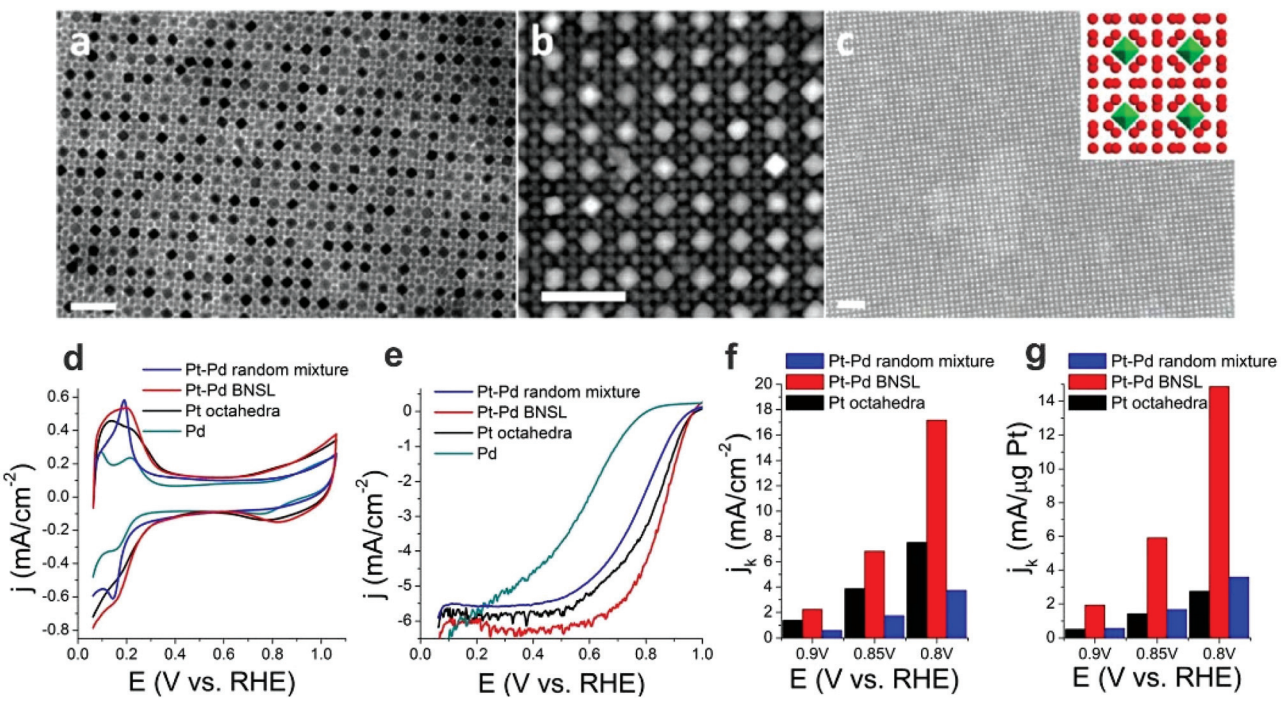

Fig. 7 (a) TEM, (b) STEM-HAADF, and (c) SEM images of Pt–Pd AB_{13}-type BN-SL. (d) Cyclic voltammogram curves and (e) oxygen reduction reaction polarization curves of a Pt–Pd BN-SL, a random mixture of Pt–Pd NCs, Pd NCs and Pt octahedra. (f) and (g) Bar chart of the kinetic current of Pt–Pd BN-SLs, a random mixture of Pt–Pd NCs, and Pt octahedra at 0.9, 0.85, and 0.8 V. Scale bars: (a) and (b) 50 nm, (c) 100 nm. Reproduced with permission from ref. 96.

Published on 18 April 2016. Downloaded by Brown University on 18/05/2016 14:35:03.

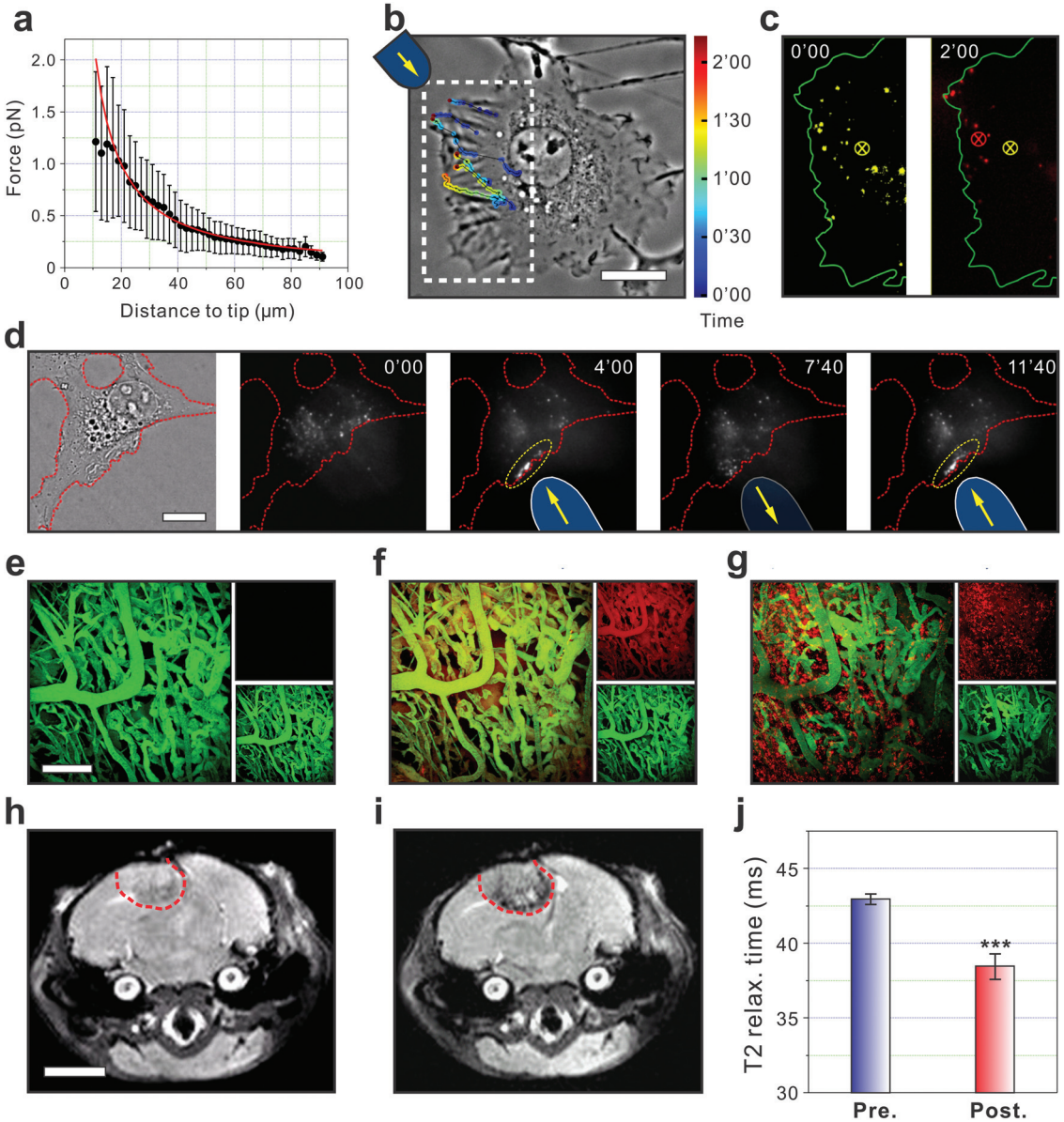

Fig. 8 Silica-coated core–shell SPs (silica-CS-SPs) in biological applications. (a) Force applied to individual silica-CS-SPs as a function of the distance from the magnetic tip. A power law (red curve) fits the data. (b) Tracking of individual silica-CS-SPs during their manipulation inside a Cos7 cell. Positions along each trajectory are color-coded according to the time. Scale bar, 15 mm. (c) Left: fluorescence imaging of individual silica-CS-SPs (yellow) in the dashed line region of (b) and before the manipulation. The barycenter of the individual localizations is shown as a yellow cross. Right: superposition of the silica-CS-SPs fluorescence after 2 min (red), the barycenter of the individual localizations is shown as a red cross. (d) Left: transmission picture of a HeLa cell in which silica-CS-SPs have been microinjected. By bringing the magnetic tip in and out (blue bars), a reversible accumulation of silica-CS-SPs (yellow region) can be created at the cell periphery (indicated by a red dashed line), in the direction of the magnet. Scale bar, 15 mm. mPEG-silane (MW5000) functionalized silica-CS-SPs (200 ml, 2 mg ml^{-1}) were intravenously injected into C3H mice bearing brain metastasis of a murine mammary carcinoma (MCaIV) with a cranial window model. Intravital multiphoton microscopy through the cranial window was carried out at different time points: pre-injection (e), 4 h post injection (f) and 24 h post injection (g). Scale bar, 150 mm. Images from red and green channels are shown in small panels (top: red channel, bottom: green channel). Green emission signals are generated from a blood vessel tracer (fluorescein isothiocyanate–dextran (FITC–Dextran)) and red emission signals are generated by mPEG-functionalized silica-CS-SPs. *In vivo* *T*2-weighted magnetic resonance images of pre- (h) and 24 h post- (i) injection of mPEG-silane functionalized silica-CS-SPs. The twenty-four hours post-injection image shows clear tumor visualization (denoted by a red dash line). Scale bar, 3 mm. (j) The corresponding *T*2 relaxation (relax.) time fitting results for the tumor region at time points of pre-injection (Pre., blue bar) and 24 h post injection (Post., red bar). n = 5 mice, ***$P < 0.001$ (Student's t-test). Reproduced with permission from ref. 36.

This journal is © The Royal Society of Chemistry 2016

Published on 18 April 2016. Downloaded by Brown University on 18/05/2016 14:35:03.

4.5 Multi-functionality

Finally, a direct advantage of combing multi-type NCs is that the fabricated materials can inherit multiple functionalities from its individual components. This multi-functionality has been highlighted in colloidal binary SP systems.[67,124] Zhang *et al.* synthesized Au–Fe_3O_4 binary SPs that displayed a combined property of magnetism and catalysis, which could be potentially used as recoverable catalysts through magnetic separation and collection.[67] Similar ideas have been applied for making QD-Fe_3O_4 binary magneto-fluorescent SPs.[68,109,125] Recently, Chen *et al.* demonstrated an excellent example of using the magneto-fluorescent 'core–shell' SPs in biological applications.[36] Given the ideal superstructure of a close-packed magnetic 'core', which is fully surrounded by a 'shell' of fluorescent QDs, the SPs exhibit uniform and tunable sizes, optimized fluorescent and magnetic properties, substantial colloidal stability as well as versatile surface functionality. These features allow the obtained SPs to be magnetically manipulated inside a living cell, while being optically tracked with a high accuracy at the single-SP level (Fig. 8a–d). With desired decorations, these SPs constitute a powerful platform for the study of intracellular processes under magnetic manipulation. Moreover, given the enhanced magnetic resonance (MR) transverse relaxivity (*i.e.*, r_2) due to the high degree of Fe_3O_4 NCs aggregation as well as their self-ordering, the SPs can also be utilized as *in vivo* MR and multiphoton dual-mode imaging probes for tumor detection and visualization at both microscopic and macroscopic scales (Fig. 8e–j).[36]

5. Conclusion and future perspectives

In this minireview, we summarized the recent advances of NC-based MCSs. We explored the general strategies employed for synthesizing MSCs, the types of NC-based superstructures, and exciting properties of these materials. It is also noteworthy to mention that advanced techniques, including 3D tomography electron microscopy with atomic resolution,[90,126] external pressure treatments and the simultaneous collection of wide- and small-angle X-ray scattering,[98,127,128] synchrotron-based X-ray supercrystallography,[129–132] along with improved theoretical modeling and simulations, have together provided a more in-depth understanding of these complicated systems from different aspects.[62,133,134] Moreover, post-processing (*e.g.*, pressure sintering), which has been recently employed for single-component superstructures,[135–137] can be easily transferred to well-defined MCSs to generate novel materials with undiscovered properties.

In the past decade, a significant amount of research has yielded plentiful discoveries in this rapidly growing field and the potential of MCSs has been unambiguously demonstrated. Despite this progress, limitations and challenges still remain. For example, a detailed understanding of the nucleation and growth processes of these MSCs has not been clearly demonstrated. BN- and TN-SL structures in robust and post-treatable forms have yet been reliably synthesized. Controlling the inter-particle distance inside MCSs in a wide range, and scalable syntheses of these materials at a manufacturing level are both quite challenging due to the delicate synthetic procedures currently used. Moreover, the properties and applications of MCSs are still far from being fully explored and studied. However, given the history of continuous progress and vast achievements in the nano-material research field, there is no doubt that these current limitations and challenges delineated by researchers will be overcome as more discoveries are made. We hope that this minireview will inspire researchers to bring multidisciplinary expertise into this young and fascinating field, and to innovatively expand the existing material–property library to push MCSs forward toward their bright future.

Acknowledgements

O.C. acknowledges support from a Brown University startup.

References

1 R. F. Gibson, A review of recent research on mechanics of multifunctional composite materials and structures, *Compos. Struct.*, 2010, **92**, 2793–2810.
2 W. H. Suh, Y. H. Suh and G. D. Stucky, Multifunctional nanosystems at the interface of physical and life sciences, *Nano Today*, 2009, **4**, 27–36.
3 N. C. Bigall, W. J. Parak and D. Dorfs, Fluorescent, magnetic and plasmonic-hybrid multifunctional colloidal nano objects, *Nano Today*, 2012, **7**, 282–296.
4 J. E. Lee, N. Lee, T. Kim, J. Kim and T. Hyeon, Multifunctional mesoporous silica nanocomposite nanoparticles for theranostic applications, *Acc. Chem. Res.*, 2011, **44**, 893–902.
5 M. D. Bentzon, J. Vanwonterghem, S. Morup, A. Tholen and C. J. W. Koch, Ordered aggregates of ultrafine iron-oxide particles - super crystals, *Philos. Mag. B*, 1989, **60**, 169–178.
6 W. Shenton, D. Pum, U. B. Sleytr and S. Mann, Synthesis of cadmium sulphide superlattices using self-assembled bacterial S-layers, *Nature*, 1997, **389**, 585–587.
7 S. Y. Park, *et al.*, DNA-programmable nanoparticle crystallization, *Nature*, 2008, **451**, 553–556.
8 F. X. Redl, K. S. Cho, C. B. Murray and S. O'Brien, Three-dimensional binary superlattices of magnetic nanocrystals and semiconductor quantum dots, *Nature*, 2003, **423**, 968–971.
9 C. J. Kiely, J. Fink, M. Brust, D. Bethell and D. J. Schiffrin, Spontaneous ordering of bimodal ensembles of nanoscopic gold clusters, *Nature*, 1998, **396**, 444–446.
10 A. E. Saunders and B. A. Korgel, Observation of an AB phase in bidisperse nanocrystal superlattices, *ChemPhysChem*, 2005, **6**, 61–65.

Published on 18 April 2016. Downloaded by Brown University on 18/05/2016 14:35:03.

11 S. C. Glotzer and M. J. Solomon, Anisotropy of building blocks and their assembly into complex structures, *Nat. Mater.*, 2007, **6**, 557–562.
12 H. Zeng, J. Li, J. P. Liu, Z. L. Wang and S. H. Sun, Exchange-coupled nanocomposite magnets by nanoparticle self-assembly, *Nature*, 2002, **420**, 395–398.
13 J. Kolny, A. Kornowski and H. Weller, Self-organization of cadmium sulfide and gold nanoparticles by electrostatic interaction, *Nano Lett.*, 2002, **2**, 361–364.
14 T. H. Galow, A. K. Boal and V. M. Rotello, A "building block" approach to mixed-colloid systems through electrostatic self-organization, *Adv. Mater.*, 2000, **12**, 576–579.
15 E. C. Hao, *et al.*, Assembly of alternating TiO_2/CdS nanoparticle composite films, *J. Mater. Chem.*, 1998, **8**, 1327–1328.
16 S. Gomez, *et al.*, Platinum colloids stabilized by bifunctional ligands: self-organization and connection to gold, *Chem. Commun.*, 2001, 1474–1475.
17 S. Fullam, H. Rensmo, S. N. Rao and D. Fitzmaurice, Noncovalent self-assembly of silver and gold nanocrystal aggregates in solution, *Chem. Mater.*, 2002, **14**, 3643–3650.
18 J. Park, J. Joo, S. G. Kwon, Y. Jang and T. Hyeon, Synthesis of monodisperse spherical nanocrystals, *Angew. Chem., Int. Ed.*, 2007, **46**, 4630–4660.
19 P. Reiss, M. Protiere and L. Li, Core/Shell Semiconductor Nanocrystals, *Small*, 2009, **5**, 154–168.
20 J. Park, *et al.*, Ultra-large-scale syntheses of monodisperse nanocrystals, *Nat. Mater.*, 2004, **3**, 891–895.
21 O. Chen, *et al.*, Compact high-quality CdSe-CdS core–shell nanocrystals with narrow emission linewidths and suppressed blinking, *Nat. Mater.*, 2013, **12**, 445–451.
22 O. Chen, H. Wei, A. Maurice, M. Bawendi and P. Reiss, Pure colors from core–shell quantum dots, *MRS Bull.*, 2013, **38**, 696–702.
23 R. Tan, *et al.*, Reducing competition by coordinating solvent promotes morphological control in alternating layer growth of CdSe/CdS core/shell quantum dots, *Chem. Mater.*, 2015, **27**, 7468–7480.
24 Y. Lalatonne, J. Richardi and M. P. Pileni, van der Waals versus dipolar forces controlling mesoscopic organizations of magnetic nanocrystals, *Nat. Mater.*, 2004, **3**, 121–125.
25 E. V. Shevchenko, D. V. Talapin, N. A. Kotov, S. O'Brien and C. B. Murray, Structural diversity in binary nanoparticle superlattices, *Nature*, 2006, **439**, 55–59.
26 A. M. Kalsin, *et al.*, Electrostatic self-assembly of binary nanoparticle crystals with a diamond-like lattice, *Science*, 2006, **312**, 420–424.
27 M. A. Kostiainen, *et al.*, Electrostatic assembly of binary nanoparticle superlattices using protein cages, *Nat. Nanotechnol.*, 2013, **8**, 52–56.
28 W. H. Evers, *et al.*, Entropy-driven formation of binary semiconductor-nanocrystal superlattices, *Nano Lett.*, 2010, **10**, 4235–4241.
29 M. I. Bodnarchuk, M. V. Kovalenko, W. Heiss and D. V. Talapin, Energetic and entropic contributions to self-assembly of binary nanocrystal superlattices: temperature as the structure-directing factor, *J. Am. Chem. Soc.*, 2010, **132**, 11967–11977.
30 Z. Yang, J. Wei, P. Bonville and M. P. Pileni, Beyond entropy: magnetic forces induce formation of quasicrystalline structure in binary nanocrystal superlattices, *J. Am. Chem. Soc.*, 2015, **137**, 4487–4493.
31 Z. D. Lu and Y. D. Yin, Colloidal nanoparticle clusters: functional materials by design, *Chem. Soc. Rev.*, 2012, **41**, 6874–6887.
32 T. Wang, D. LaMontagne, J. Lynch, J. Q. Zhuang and Y. C. Cao, Colloidal superparticles from nanoparticle assembly, *Chem. Soc. Rev.*, 2013, **42**, 2804–2823.
33 D. Nykypanchuk, M. M. Maye, D. van der Lelie and O. Gang, DNA-guided crystallization of colloidal nanoparticles, *Nature*, 2008, **451**, 549–552.
34 R. J. Macfarlane, *et al.*, Nanoparticle superlattice engineering with DNA, *Science*, 2011, **334**, 204–208.
35 A. G. Dong, J. Chen, P. M. Vora, J. M. Kikkawa and C. B. Murray, Binary nanocrystal superlattice membranes self-assembled at the liquid-air interface, *Nature*, 2010, **466**, 474–477.
36 O. Chen, *et al.*, Magneto-fluorescent core–shell supernanoparticles, *Nat. Commun.*, 2014, **5**, 5093.
37 J. J. Urban, D. V. Talapin, E. V. Shevchenko, C. R. Kagan and C. B. Murray, Synergism in binary nanocrystal superlattices leads to enhanced p-type conductivity in self-assembled PbTe/Ag_2Te thin films, *Nat. Mater.*, 2007, **6**, 115–121.
38 Y. Zhang, F. Lu, K. G. Yager, D. van der Lelie and O. Gang, A general strategy for the DNA-mediated self-assembly of functional nanoparticles into heterogeneous systems, *Nat. Nanotechnol.*, 2013, **8**, 865–872.
39 D. V. Talapin, J. S. Lee, M. V. Kovalenko and E. V. Shevchenko, Prospects of colloidal nanocrystals for electronic and optoelectronic applications, *Chem. Rev.*, 2010, **110**, 389–458.
40 Z. Nie, A. Petukhova and E. Kumacheva, Properties and emerging applications of self-assembled structures made from inorganic nanoparticles, *Nat. Nanotechnol.*, 2010, **5**, 15–25.
41 M. V. Kovalenko, *et al.*, Prospects of nanoscience with nanocrystals, *ACS Nano*, 2015, **9**, 1012–1057.
42 T. Hanrath, Colloidal nanocrystal quantum dot assemblies as artificial solids, *J. Vac. Sci. Technol., A*, 2012, **30**, 030802.
43 C. Y. Wang, C. Siu, J. Zhang and J. Y. Fang, Understanding the forces acting in self-assembly and the implications for constructing three-dimensional (3D) supercrystals, *Nano Res.*, 2015, **8**, 2445–2466.
44 D. Luo, C. Yan and T. Wang, Interparticle forces underlying nanoparticle self-assemblies, *Small*, 2015, **11**, 5984–6008.
45 Z. W. Quan and J. Y. Fang, Superlattices with non-spherical building blocks, *Nano Today*, 2010, **5**, 390–411.

 This journal is © The Royal Society of Chemistry 2016

Published on 18 April 2016. Downloaded by Brown University on 18/05/2016 14:35:03.

46 P. C. Ohara, D. V. Leff, J. R. Heath and W. M. Gelbart, Crystallization of opals from polydisperse nanoparticles, *Phys. Rev. Lett.*, 1995, **75**, 3466–3469.
47 M. D. Eldridge, P. A. Madden and D. Frenkel, Entropy-driven formation of a superlattice in hardsphere binary mixture, *Nature*, 1993, **365**, 35–37.
48 X. Cottin and P. A. Monson, Substitutionally ordered solid-solutions of hard-spheres, *J. Chem. Phys.*, 1995, **102**, 3354–3360.
49 P. G. Bolhuis, D. Frenkel, S. C. Mau and D. A. Huse, Entropy difference between crystal phases, *Nature*, 1997, **388**, 235–236.
50 E. Trizac, M. D. Eldridge and P. A. Madden, Stability of the AB crystal for asymmetric binary hard sphere mixtures, *Mol. Phys.*, 1997, **90**, 675–678.
51 Z. Chen, J. Moore, G. Radtke, H. Sirringhaus and S. O'Brien, Binary nanoparticle superlattices in the semiconductor-semiconductor system: CdTe and CdSe, *J. Am. Chem. Soc.*, 2007, **129**, 15702–15709.
52 E. V. Shevchenko, D. V. Talapin, C. B. Murray and S. O'Brien, Structural characterization of self-assembled multifunctional binary nanoparticle superlattices, *J. Am. Chem. Soc.*, 2006, **128**, 3620–3637.
53 A. Dong, J. Chen, X. Ye, J. M. Kikkawa and C. B. Murray, Enhanced thermal stability and magnetic properties in NaCl-type FePt-MnO binary nanocrystal superlattices, *J. Am. Chem. Soc.*, 2011, **133**, 13296–13299.
54 A. Dong, X. Ye, J. Chen and C. B. Murray, Two-dimensional binary and ternary nanocrystal superlattices: the case of monolayers and bilayers, *Nano Lett.*, 2011, **11**, 1804–1809.
55 M. Cargnello, B. T. Diroll, E. A. Gaulding and C. B. Murray, Enhanced energy transfer in quasi-quaternary nanocrystal superlattices, *Adv. Mater.*, 2014, **26**, 2419–2423.
56 Y. Yamada, *et al.*, Nanocrystal bilayer for tandem catalysis, *Nat. Chem.*, 2011, **3**, 372–376.
57 X. Ye, *et al.*, Structural diversity in binary superlattices self-assembled from polymer-grafted nanocrystals, *Nat. Commun.*, 2015, **6**, 10052.
58 P. Li, Z. Wei, T. Wu, Q. Peng and Y. Li, Au-ZnO hybrid nanopyramids and their photocatalytic properties, *J. Am. Chem. Soc.*, 2011, **133**, 5660–5663.
59 M. A. Boles and D. V. Talapin, Many-body effects in nanocrystal superlattices: departure from sphere packing explains stability of binary phases, *J. Am. Chem. Soc.*, 2015, **137**, 4494–4502.
60 J. Wei, N. Schaeffer and M. P. Pileni, Ligand exchange governs the crystal structures in binary nanocrystal superlattices, *J. Am. Chem. Soc.*, 2015, **137**, 14773–14784.
61 V. Liljestrom, J. Mikkila and M. A. Kostiainen, Self-assembly and modular functionalization of three-dimensional crystals from oppositely charged proteins, *Nat. Commun.*, 2014, **5**, 4445.
62 E. Auyeung, *et al.*, DNA-mediated nanoparticle crystallization into Wulff polyhedra, *Nature*, 2014, **505**, 73–77.
63 C. Zhang, *et al.*, A general approach to DNA-programmable atom equivalents, *Nat. Mater.*, 2013, **12**, 741–746.
64 Y. Zhang, *et al.*, Selective transformations between nanoparticle superlattices via the reprogramming of DNA-mediated interactions, *Nat. Mater.*, 2015, **14**, 840–847.
65 S. Zhang, Y. Y. Shao, G. P. Yin and Y. H. Lin, Electrostatic self-assembly of a Pt-around-Au nanocomposite with high activity towards formic acid oxidation, *Angew. Chem., Int. Ed.*, 2010, **49**, 2211–2214.
66 F. Bai, *et al.*, A versatile bottom-up assembly approach to colloidal spheres from nanocrystals, *Angew. Chem., Int. Ed.*, 2007, **46**, 6650–6653.
67 X. Zhang, *et al.*, Binary superparticles from preformed Fe_3O_4 and Au nanoparticles, *CrystEngComm*, 2011, **13**, 5674–5676.
68 J. S. Han, *et al.*, Fabrication of CdTe nanoparticles-based superparticles for an improved detection of Cu^{2+} and Ag^{+}, *J. Mater. Chem.*, 2012, **22**, 2679–2686.
69 Z. D. Lu, M. M. Ye, N. Li, W. W. Zhong and Y. D. Yin, Self-assembled TiO_2 nanocrystal clusters for selective enrichment of intact phosphorylated proteins, *Angew. Chem., Int. Ed.*, 2010, **49**, 1862–1866.
70 J. Q. Zhuang, H. M. Wu, Y. G. Yang and Y. C. Cao, Controlling colloidal superparticle growth through solvophobic interactions, *Angew. Chem., Int. Ed.*, 2008, **47**, 2208–2212.
71 J. Zhuang, H. Wu, Y. Yang and Y. C. Cao, Supercrystalline colloidal particles from artificial atoms, *J. Am. Chem. Soc.*, 2007, **129**, 14166–14167.
72 J. Zhuang, *et al.*, Cylindrical superparticles from semiconductor nanorods, *J. Am. Chem. Soc.*, 2009, **131**, 6084–6085.
73 T. Wang, *et al.*, Self-assembled colloidal superparticles from nanorods, *Science*, 2012, **338**, 358–363.
74 Z. Yang, *et al.*, Supracrystalline colloidal eggs: epitaxial growth and freestanding three-dimensional supracrystals in nanoscaled colloidosomes, *J. Am. Chem. Soc.*, 2016, **138**, 3493–3500.
75 J. Wei, *et al.*, Yolk/Shell assembly of gold nanoparticles by size segregation in solution, *J. Am. Chem. Soc.*, 2016, **138**, 3274–3277.
76 C. J. Kiely, *et al.*, Ordered colloidal nanoalloys, *Adv. Mater.*, 2000, **12**, 640–643.
77 E. V. Shevchenko, D. V. Talapin, S. O'Brien and C. B. Murray, Polymorphism in AB_{13} nanoparticle superlattices an example of semiconductor-metal metamaterials, *J. Am. Chem. Soc.*, 2005, **127**, 8741–8747.
78 E. Auyeung, *et al.*, Synthetically programmable nanoparticle superlattices using a hollow three-dimensional spacer approach, *Nat. Nanotechnol.*, 2012, **7**, 24–28.
79 R. J. Macfarlane, M. R. Jones, B. Lee, E. Auyeung and C. A. Mirkin, Topotactic interconversion of nanoparticle superlattices, *Science*, 2013, **341**, 1222–1225.
80 F. Lu, K. G. Yager, Y. Zhang, H. Xin and O. Gang, Superlattices assembled through shape-induced directional binding, *Nat. Commun.*, 2015, **6**, 6912.
81 E. V. Shevchenko, J. B. Kortright, D. V. Talapin, S. Aloni and A. P. Alivisatos, Quasi-ternary nanoparticle super-

Published on 18 April 2016. Downloaded by Brown University on 18/05/2016 14:35:03.

lattices through nanoparticle design, *Adv. Mater.*, 2007, **19**, 4183–4188.
82 E. V. Shevchenko, *et al.*, Self-assembled binary superlattices of CdSe and Au nanocrystals and their fluorescence properties, *J. Am. Chem. Soc.*, 2008, **130**, 3274–3275.
83 C. Lu, Z. Chen and S. O'Brien, Optimized conditions for the self-organization of CdSe-Au and CdSe-CdSe binary nanoparticle superlattices, *Chem. Mater.*, 2008, **20**, 3594–3600.
84 Z. Chen and S. O'Brien, Structure direction of II-VI semiconductor quantum dot binary nanoparticle superlattices by tuning radius ratio, *ACS Nano*, 2008, **2**, 1219–1229.
85 K. Overgaag, *et al.*, Binary superlattices of PbSe and CdSe nanocrystals, *J. Am. Chem. Soc.*, 2008, **130**, 7833–7835.
86 X. Ye, J. Chen and C. B. Murray, Polymorphism in self-assembled AB_6 binary nanocrystal superlattices, *J. Am. Chem. Soc.*, 2011, **133**, 2613–2620.
87 A. B. Schofield, Binary hard-sphere crystals with the cesium chloride structure, *Phys. Rev. E: Stat., Nonlinear, Soft Matter Phys.*, 2001, **64**, 051403.
88 Z. Yang, J. Wei and M. P. Pileni, Metal–Metal binary nanoparticle superlattices: a case study of mixing Co and Ag nanoparticles, *Chem. Mater.*, 2015, **27**, 2152–2157.
89 Z. Yang, J. Wei, P. Bonville and M. P. Pileni, Engineering the magnetic dipolar interactions in 3D binary supracrystals via mesoscale alloying, *Adv. Funct. Mater.*, 2015, **25**, 4908–4915.
90 M. P. Boneschanscher, *et al.*, Electron tomography resolves a novel crystal structure in a binary nanocrystal superlattice, *Nano Lett.*, 2013, **13**, 1312–1316.
91 D. V. Talapin, *et al.*, Quasicrystalline order in self-assembled binary nanoparticle superlattices, *Nature*, 2009, **461**, 964–967.
92 M. I. Bodnarchuk, E. V. Shevchenko and D. V. Talapin, Structural defects in periodic and quasicrystalline binary nanocrystal superlattices, *J. Am. Chem. Soc.*, 2011, **133**, 20837–20849.
93 A. Sanchez-Iglesias, M. Grzelczak, J. Perez-Juste and L. M. Liz-Marzan, Binary self-assembly of gold nanowires with nanospheres and nanorods, *Angew. Chem., Int. Ed.*, 2010, **49**, 9985–9989.
94 Y. Nagaoka, T. Wang, J. Lynch, D. LaMontagne and Y. C. Cao, Binary assembly of colloidal semiconductor nanorods with spherical metal nanoparticles, *Small*, 2012, **8**, 843–846.
95 X. Ye, *et al.*, Shape alloys of nanorods and nanospheres from self-assembly, *Nano Lett.*, 2013, **13**, 4980–4988.
96 Y. Kang, *et al.*, Design of Pt-Pd binary superlattices exploiting shape effects and synergistic effects for oxygen reduction reactions, *J. Am. Chem. Soc.*, 2013, **135**, 42–45.
97 T. Paik and C. B. Murray, Shape-directed binary assembly of anisotropic nanoplates: a nanocrystal puzzle with shape-complementary building blocks, *Nano Lett.*, 2013, **13**, 2952–2956.
98 W. H. Evers, H. Friedrich, L. Filion, M. Dijkstra and D. Vanmaekelbergh, Observation of a ternary nanocrystal superlattice and its structural characterization by electron tomography, *Angew. Chem., Int. Ed.*, 2009, **48**, 9655–9657.
99 T. Paik, B. T. Diroll, C. R. Kagan and C. B. Murray, Binary and ternary superlattices self-assembled from colloidal nanodisks and nanorods, *J. Am. Chem. Soc.*, 2015, **137**, 6662–6669.
100 P. Podsiadlo, *et al.*, The role of order, nanocrystal size, and capping ligands in the collective mechanical response of three-dimensional nanocrystal solids, *J. Am. Chem. Soc.*, 2010, **132**, 8953–8960.
101 S. M. Rupich, E. V. Shevchenko, M. I. Bodnarchuk, B. Lee and D. V. Talapin, Size-dependent multiple twinning in nanocrystal superlattices, *J. Am. Chem. Soc.*, 2010, **132**, 289–296.
102 O. C. Compton and F. E. Osterloh, Evolution of size and shape in the colloidal crystallization of gold nanoparticles, *J. Am. Chem. Soc.*, 2007, **129**, 7793–7798.
103 M. R. Jones, *et al.*, DNA-nanoparticle superlattices formed from anisotropic building blocks, *Nat. Mater.*, 2010, **9**, 913–917.
104 B. Radha, *et al.*, Reconstitutable nanoparticle superlattices, *Nano Lett.*, 2014, **14**, 2162–2167.
105 M. B. Ross, J. C. Ku, V. M. Vaccarezza, G. C. Schatz and C. A. Mirkin, Nanoscale form dictates mesoscale function in plasmonic DNA-nanoparticle superlattices, *Nat. Nanotechnol.*, 2015, **10**, 453–458.
106 C. A. Mirkin, R. L. Letsinger, R. C. Mucic and J. J. Storhoff, A DNA-based method for rationally assembling nanoparticles into macroscopic materials, *Nature*, 1996, **382**, 607–609.
107 S. J. Park, A. A. Lazarides, J. J. Storhoff, L. Pesce and C. A. Mirkin, The structural characterization of oligonucleotide-modified gold nanoparticle networks formed by DNA hybridization, *J. Phys. Chem. B*, 2004, **108**, 12375–12380.
108 C. Chen, *et al.*, Mesoporous multicomponent nanocomposite colloidal spheres: ideal high-temperature stable model catalysts, *Angew. Chem., Int. Ed.*, 2011, **50**, 3725–3729.
109 D. H. Ortgies, *et al.*, In vivo deep tissue fluorescence and magnetic imaging employing hybrid nanostructures, *ACS Appl. Mater. Interfaces*, 2016, **8**, 1406–1414.
110 Q. Zhang, X. Wang and Y. Zhu, Multicolor upconverted luminescence-encoded superparticles via controlling self-assembly based on hydrophobic lanthanide-doped $NaYF_4$ nanocrystals, *J. Mater. Chem.*, 2011, **21**, 12132–12138.
111 D. Nepal, L. F. Drummy, S. Biswas, K. Park and R. A. Vaia, Large scale solution assembly of quantum dot–gold nanorod architectures with plasmon enhanced fluorescence, *ACS Nano*, 2013, **7**, 9064–9074.
112 E. Cohen-Hoshen, G. W. Bryant, I. Pinkas, J. Sperling and I. Bar-Joseph, Exciton-plasmon interactions in quantum dot-gold nanoparticle structures, *Nano Lett.*, 2012, **12**, 4260–4264.
113 D. Z. Sun, *et al.*, Light-harvesting nanoparticle core–shell clusters with controllable optical output, *ACS Nano*, 2015, **9**, 5657–5665.

 This journal is © The Royal Society of Chemistry 2016

Published on 18 April 2016. Downloaded by Brown University on 18/05/2016 14:35:03.

114 R. Schreiber, *et al.*, Hierarchical assembly of metal nanoparticles, quantum dots and organic dyes using DNA origami scaffolds, *Nat. Nanotechnol.*, 2014, **9**, 74–78.
115 K. Ma, O. Yehezkeli, D. W. Domaille, H. H. Funke and J. N. Cha, Enhanced hydrogen production from DNA-assembled Z-scheme TiO_2-CdS photocatalyst systems, *Angew. Chem., Int. Ed.*, 2015, **54**, 11490–11494.
116 J. Chen, *et al.*, Bistable magnetoresistance switching in exchange-coupled $CoFe_2O_4$-Fe_3O_4 binary nanocrystal superlattices by self-assembly and thermal annealing, *ACS Nano*, 2013, **7**, 1478–1486.
117 Y. Kang, *et al.*, Engineering catalytic contacts and thermal stability: gold/iron oxide binary nanocrystal superlattices for CO oxidation, *J. Am. Chem. Soc.*, 2013, **135**, 1499–1505.
118 S. Dey, *et al.*, An experimental and theoretical mechanistic study of biexciton quantum yield enhancement in single quantum dots near gold nanoparticles, *Nanoscale*, 2015, **7**, 6851–6858.
119 B. Ji, *et al.*, Non-blinking quantum dot with a plasmonic nanoshell resonator, *Nat. Nanotechnol.*, 2015, **10**, 170–175.
120 K. T. Shimizu, W. K. Woo, B. R. Fisher, H. J. Eisler and M. G. Bawendi, Surface-enhanced emission from single semiconductor nanocrystals, *Phys. Rev. Lett.*, 2002, **89**, 117401.
121 X. Li, F. J. Kao, C. C. Chuang and S. He, Enhancing fluorescence of quantum dots by silica-coated gold nanorods under one- and two-photon excitation, *Opt. Express*, 2010, **18**, 11335–11346.
122 X. Ye, J. Chen, B. T. Diroll and C. B. Murray, Tunable plasmonic coupling in self-assembled binary nanocrystal superlattices studied by correlated optical microspectrophotometry and electron microscopy, *Nano Lett.*, 2013, **13**, 1291–1297.
123 T. Zheng, *et al.*, Construction of $NaREF_4$-based binary and bilayer nanocrystal assemblies, *Chem. Commun.*, 2013, **49**, 5799–5801.
124 G. L. Yang, H. Z. Zhong, R. B. Liu, Y. F. Li and B. S. Zou, In situ aggregation of ZnSe nanoparticles into supraparticles: shape control and doping effects, *Langmuir*, 2013, **29**, 1970–1976.
125 X. Y. Sun, *et al.*, Bifunctional superparticles achieved by assembling fluorescent $CuInS_2$@ZnS quantum dots and amphibious Fe_3O_4 nanocrystals, *J. Phys. Chem. C*, 2013, **117**, 21014–21020.
126 S. Bals, B. Goris, L. M. Liz-Marzan and G. Van Tendeloo, Three-dimensional characterization of noble-metal nanoparticles and their assemblies by electron tomography, *Angew. Chem., Int. Ed.*, 2014, **53**, 10600–10610.
127 H. Wu, Z. Wang and H. Fan, Stress-induced nanoparticle crystallization, *J. Am. Chem. Soc.*, 2014, **136**, 7634–7636.
128 Z. Wang, *et al.*, Integrating in situ high pressure small and wide angle synchrotron x-ray scattering for exploiting new physics of nanoparticle supercrystals, *Rev. Sci. Instrum.*, 2010, **81**, 093902.
129 Z. Wang, *et al.*, Correlating superlattice polymorphs to internanoparticle distance, packing density, and surface lattice in assemblies of PbS nanoparticles, *Nano Lett.*, 2013, **13**, 1303–1311.
130 R. Li, K. Bian, T. Hanrath, W. A. Bassett and Z. Wang, Decoding the superlattice and interface structure of truncate PbS nanocrystal-assembled supercrystal and associated interaction forces, *J. Am. Chem. Soc.*, 2014, **136**, 12047–12055.
131 R. Li, *et al.*, An obtuse rhombohedral superlattice assembled by Pt nanocubes, *Nano Lett.*, 2015, **15**, 6254–6260.
132 R. Li, *et al.*, Competing interactions between various entropic forces toward assembly of Pt_3Ni octahedra into a body-centered cubic superlattice, *Nano Lett.*, 2016, **16**, 2792–2799.
133 P. F. Damasceno, M. Engel and S. C. Glotzer, Predictive self-assembly of polyhedra into complex structures, *Science*, 2012, **337**, 453–457.
134 M. R. Khadilkar and F. A. Escobedo, Heuristic rule for binary superlattice coassembly: mixed plastic mesophases of hard polyhedral nanoparticles, *Phys. Rev. Lett.*, 2014, **113**, 165504.
135 H. Wu, *et al.*, Nanostructured gold architectures formed through high pressure-driven sintering of spherical nanoparticle arrays, *J. Am. Chem. Soc.*, 2010, **132**, 12826–12828.
136 Z. Wang, *et al.*, Deviatoric stress driven formation of large single-crystal PbS nanosheet from nanoparticles and in situ monitoring of oriented attachment, *J. Am. Chem. Soc.*, 2011, **133**, 14484–14487.
137 T. Wang, *et al.*, Pressure processing of nanocube assemblies toward harvesting of a metastable PbS phase, *Adv. Mater.*, 2015, **27**, 4544–4549.
138 Y. Sakamoto, *et al.*, Electron Microscopy Study of Binary Nanocolloidal Crystals with ico-AB_{13} Structure Made of Monodisperse Silica Nanoparticles, *J. Phys. Chem. C*, 2014, **118**, 15004–15010.
139 M. I. Bodnarchuk, R. Erni, F. Krumeich and M. V. Kovalenko, Binary superlattices from colloidal nanocrystals and giant polyoxometalate clusters, *Nano Lett.*, 2013, **13**, 1699–1705.
140 R. Breitwieser, *et al.*, Binary superlattices from $\{Mo_{132}\}$ polyoxometalates and maghemite nanocrystals: long-range ordering and fine-tuning of dipole interactions, *Small*, 2016, **12**, 220–228.
141 T. Altantzis, Z. Yang, S. Bals, G. Van Tendeloo and M.-P. Pileni, Thermal stability of $CoAu_{13}$ binary nanoparticle superlattices under the electron beam, *Chem. Mater.*, 2016, **28**, 716–719.
142 B. E. Treml, B. Lukose, P. Clancy, D. M. Smilgies and T. Hanrath, Connecting the particles in the box-controlled fusion of hexamer nanocrystal clusters within an AB_6 binary nanocrystal superlattice, *Sci. Rep.*, 2014, **4**, 6731.
143 Y. Yu, C. A. Bosoy, D. M. Smilgies and B. A. Korgel, Self-assembly and thermal stability of binary superlattices of gold and silicon nanocrystals, *J. Phys. Chem. Lett.*, 2013, **4**, 3677–3682.